Lanthanide Podates with Predetermined Structural and Photophysical Properties: Strongly Luminescent Self-Assembled Heterodinuclear d−f Complexes with a Segmental Ligand Containing Heterocyclic Imines and Carboxamide Binding Units

Claude Piguet,*,† Jean-Claude G. Bünzli,*,‡ Gérald Bernardinelli,§ Gérard Hopfgartner,⊥ Stéphane Petoud,‡ and Olivier Schaad||

Contribution from the Department of Inorganic, Analytical and Applied Chemistry, the Laboratory of X-ray Crystallography, and the Department of Biochemistry, University of Geneva, CH-1211 Geneva 4, Switzerland, the Institute of Analytical and Inorganic Chemistry, University of Lausanne, CH-1015 Lausanne, Switzerland, and Pharma Division, F. Hoffmann-La Roche Ltd., CH-4002 Basel, Switzerland

Received December 11, 1995[⊗]

Abstract: The segmental ligand 2-{6-[*N*,*N*-diethylcarbamoyl]pyridin-2-yl}-1,1′-dimethyl-5,5′-methylene-2′-(5-methylpyridin-2-yl)bis[1*H*-benzimidazole] (L^2) reacts with stoichiometric amounts of Ln(III) (Ln = La−Nd, Sm−Tb, Tm−Lu, Y) and Zn(II) in acetonitrile to yield quantitatively and selectively the heterodinuclear triple-helical complexes $[LnZn(L^2)_3]^{5+}$ under thermodynamic control. The crystal structure of $[EuZn(L^2)_3](ClO_4)(CF_3SO_3)_4(CH_3CN)_4$ (**13**; $EuZnC_{111}H_{111}N_{25}O_{19}F_{12}S_4Cl$, monoclinic, *C*2/*c*, *Z* = 8) shows the wrapping of the three ligands L^2 about a pseudo-C_3 axis passing through the metal ions. Zn(II) occupies the distorted pseudooctahedral capping coordination site defined by the three bidentate binding units while Eu(III) lies in the resulting "facial" pseudotricapped trigonal prismatic site produced by the three remaining tridentate units as exemplified by luminescence measurements using the Eu(III) structural probe. The separation of contact and pseudocontact contributions to the ^{1}H-NMR paramagnetic shifts of the axial complexes $[LnZn(L^2)_3]^{5+}$ (Ln = Ce, Pr, Nd, Sm, Eu, Tm, Yb) establishes that the triple helical structure is maintained in solution. Photophysical measurements and quantum yields in acetonitrile indicate that the terminal *N*,*N*-diethylcarbamoyl group in L^2 favors efficient intramolecular $L^2 \rightarrow$ Eu(III) energy transfers leading to strong Eu-centered red luminescence. Improved resistance toward hydrolysis also results from the use of carboxamide groups, and no change in luminescence is observed for $[EuZn(L^2)_3]^{5+}$ in moist acetonitrile. The preparation of the segmental ligand L^2 from the new asymmetric synthon 6-(*N*,*N*-diethylcarbamoyl)pyridine-2-carboxylic acid is described together with its crystal and molecular structure ($C_{33}H_{33}N_7O$, monoclinic, $P2_1/c$, $Z = 4$). The use of 3d metal ions as a noncovalent tripodal spacer for lanthanide podates is discussed together with the crucial role played by carboxamide groups for the control of structural, electronic, and photophysical properties.

Introduction

The design of organized molecular architectures containing lanthanide metal ions Ln(III) and working as nanometric light-converting devices[1,2] and luminescent probes[1] is a theme of considerable current interest in supramolecular[1,2] and analytical chemistry,[1,3] and biochemistry.[4] However, the selective introduction of Ln(III) into supramolecular complexes with tailored coordination sites and predetermined photophysical properties represents a synthetic challenge[5] since Ln(III) displays large and variable coordination numbers[6] with few stereochemical preferences.[6,7] The control of the coordination spheres around Ln(III) thus mainly depends on the preorganization[8] of the coordinating units which limits the structural flexibility and increases the thermodynamic stability.[9] Macrocyclic[10] and compartmental[11] Schiff bases have been systematically investigated for the preparation of homo- and heteropolynuclear lanthanide complexes, but improved structural control and protection of Ln(III) are obtained with preorganized tri- to

† Department of Inorganic, Analytical and Applied Chemistry, University of Geneva.
‡ University of Lausanne.
§ Laboratory of X-ray Crystallography, University of Geneva.
⊥ F. Hoffmann-La Roche Ltd.
|| Department of Biochemistry, University of Geneva.
⊗ Abstract published in *Advance ACS Abstracts,* July 1, 1996.

(1) Bünzli, J.-C. G. in *Lanthanide Probes in Life, Chemical and Earth Sciences*; Bünzli, J.-C. G., Choppin, G. R., Eds.; Elsevier Publishing Co.: Amsterdam, 1989; Chapter 7. Bünzli, J.-C. G.; Froidevaux, P.; Piguet, C. *New J. Chem.* **1995**, *19*, 661−668 and references therein.
(2) Sabbatini, N.; Guardigli, M.; Lehn, J.-M. *Coord. Chem. Rev.* **1993**, *123*, 201−228.
(3) Lehn, J.-M.; Regnouf de Vains, J.-B. *Helv. Chim. Acta* **1992**, *75*, 1221−1236. Richardson, F. S. *Chem. Rev.* **1982**, *82*, 541−552.
(4) Selvin, P. R.; Rana, T. M.; Hearst, J. E. *J. Am. Chem. Soc.* **1994**, *116*, 6029−6030. Coates, J.; Sammes, P. G.; West, R. M. *J. Chem. Soc., Chem. Commun.* **1995**, 1107−1108. Saha, A. K.; Kross, K.; Kloszewski, E. D.; Upson, D. A.; Toner, J. L.; Snow, R. A.; Black, C. D. V.; Desai, V. C. *J. Am. Chem. Soc.* **1993**, *115*, 11032−11033.
(5) Piguet, C.; Bünzli, J.-C. G.; Bernardinelli, G.; Hopfgartner, G.; Williams, A. F. *J. Alloys Compd.* **1995**, *225*, 324−331.
(6) Choppin, G. R. In *Lanthanide Probes in Life, Chemical and Earth Sciences*; Bünzli, J.-C. G., Choppin, G. R., Eds.; Elsevier Publishing Co.: Amsterdam, 1989; Chapter 1. Drew, M. G. B. *Coord. Chem. Rev.* **1977**, *24*, 179−275.
(7) Reisfeld, R.; Jørgensen, C. K. Lasers and Excited States of Rare Earths. *Inorganic Chemistry Concepts*; Springer Verlag: Berlin−Heidelberg−New York, 1977; Vol. 1, Chapter 1.
(8) Lehn, J.-M. *Angew. Chem., Int. Ed. Engl.* **1988**, *27*, 89−112. Cram, D. J. *Angew. Chem., Int. Ed. Engl.* **1988**, *27*, 1009−1027.
(9) Martell, A. E.; Hancock, R. D.; Motekaitis, R. J. *Coord. Chem. Rev.* **1994**, *133*, 39−65.
(10) Alexander, V. *Chem. Rev.* **1995**, *95*, 273−342 and references therein.
(11) Guerriero, P.; Tamburini, S.; Vigato, P. A. *Coord. Chem. Rev.* **1995**, *139*, 17−243 and references therein.

S0002-7863(95)04163-1 CCC: $12.00

Chart 1

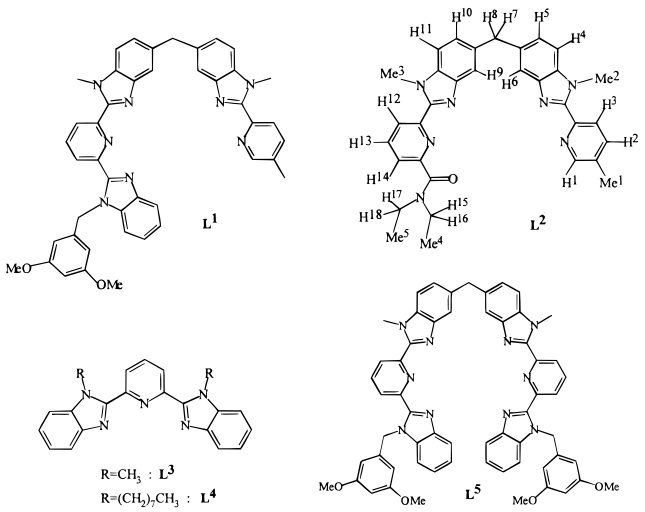

hexapodal ligands possessing iminophenolate,[12] bipyridine,[13] 1,10-phenanthroline,[14] and hydroxypyridonate[15] coordinating side arms connected to a capping covalent spacer. Further developments have led to the syntheses of rigid and highly preorganized macrobicyclic cryptands[2] possessing biheteroaryl[2,3,8] and aliphatic polyamine[16] and polyglycol[2] binding units connected to two terminal covalent tripods. Stable, strongly luminescent, and often water resistant lanthanide complexes result from the reaction of rigid cryptands with Ln(III), but the fine-tuning of the coordination cavity and of the electronic properties is severely limited by the tedious syntheses of macropolycyclic receptors.[17] Inspired by the *induced fit* concept,[18] recent studies aim to replace the covalent spacers in preorganized receptors by noncovalent d-block metal complexes which offer more synthetic and structural flexibilities and allow the possible fine-tuning of the complexation properties of the resulting receptors. For instance, α,α′-diimine binding units have been connected by two inert facial pseudooctahedral Cr(III) complexes to give an organometallic macrobicyclic cryptand.[19] Recently, two segmental ligands possessing several bidentate binding units have been assembled by a labile pseudotetrahedral Cu(I), producing a new receptor suitable for the complexation of aliphatic dicarboxylic acids.[20] The application of this concept to lanthanide chemistry has led to the development of the segmental ligand L^1 (Chart 1) which possesses a tridentate binding unit coded for Ln(III)[21] and a bidentate unit suitable for pseudooctahedral d-block metal ions.[22] L^1 reacts with a stoichiometric amount of Ln(III) (Ln = La to Lu) and Zn(II) in acetonitrile to give the heterodinuclear complexes $[LnZn(L^1)_3]^{5+}$, where Zn(II) is coordinated by the three bidentate units in a facial pseudooctahedral arrangement, producing a noncovalent tripodal spacer which controls the orientation of the remaining tridentate units, leading to a "facial" pseudotricapped trigonal prismatic site around Ln(III).[23] The fine-tuning of the structural, magnetic, and photophysical properties results from the judicious choice of the d-block metal ion,[24] and the replacement of Zn(II) by Fe(II) leads to the formation of spin-crossover heterodinuclear triple-helical complexes $[LnFe(L^1)_3]^{5+}$ for Ln = La to Eu.[24] However, the lipophilic tridentate unit of L^1 gives only amorphous solids during the isolation of the complexes, and the great similitudes between the two binding units in L^1 (same ligating atoms and bite angles) limit the selectivity of the assembly process, leading to the quantitative formation of the heterodinuclear complexes $[LnZn(L^1)_3]^{5+}$ in solution under specific conditions: (i) concentration of the ligand >0.01 M, (ii) anhydrous acetonitrile as solvent, and (iii) stoichiometric ratio $Ln:Zn:L^1 = 1:1:3$.[23,24] This, together with the faint luminescence of $[EuZn(L^1)_3]^{5+}$ resulting from the closely packed arrangement of the ligands,[21] has prompted us to replace the terminal benzimidazole group with a carboxamide group, leading to the new segmental ligand L^2 which is expected (i) to improve the selective complexation of 3d- and 4f-block metal ions,[25] (ii) to favor resonant $L^2 \rightarrow Ln$ (Ln = Eu, Tb) energy transfers,[26] and (iii) to stabilize the complexes in hydroxylic solvents.

In this paper, we present the synthesis of the new segmental ligand L^2 and the thermodynamic assembly processes leading to the strongly luminescent triple-helical heterodinuclear complexes $[LnZn(L^2)_3]^{5+}$ (Ln = La to Lu) whose crystal structure (Ln = Eu) has been partially reported in a preliminary communication.[27] Detailed photophysical studies are reported, and particular attention is focused on the structure and quantum yields in solution since these points are crucial to the design of lanthanide building blocks with predetermined structural and photophysical properties.

Experimental Section

Solvents and starting materials were purchased from Fluka AG (Buchs, Switzerland) and used without further purification, unless otherwise stated. Acetonitrile, 1,2-dichloroethane, dichloromethane, *N*,*N*-dimethylformamide (DMF), and triethylamine were distilled from CaH_2, thionyl chloride was distilled from elemental sulfur, and *N*,*N*-diethylamine was distilled from KOH. Silicagel (Merck 60, 0.040−0.060 mm) was used for preparative column chromatography.

Preparation of the Ligand. 6-Methylpyridine-2-carboxylic acid (**1**)[28] and *N*,5-dimethyl-*N*-{4′-[4″-(methylamino)-3″-nitrobenzyl]-2′-nitrophenyl}pyridine-2-carboxamide (**4**)[29] were prepared according to literature procedures.

(12) Yang, L. W.; Liu, S.; Wong, E.; Rettig, S. J.; Orvig, C. *Inorg. Chem.* **1995**, *34*, 2164−2178 and references therein.

(13) Balzani, V.; Berghmans, E.; Lehn, J.-M.; Sabbatini, N.; Terörde, R.; Ziessel, R. *Helv. Chim. Acta* **1990**, *73*, 2083−2089. Ziessel, R.; Maestri, M.; Prodi, L.; Balzani, V.; Van Doersselaer, A. *Inorg. Chem.* **1993**, *32*, 1237−1241.

(14) Sabbatini, N.; Guardigli, M.; Manet, I.; Bolleta, F.; Ziessel, R. *Inorg. Chem.* **1994**, *33*, 955−959.

(15) Xu, J.; Franklin, S. J.; Whisenhunt, D. W.; Raymond, K. N.; *J. Am. Chem. Soc.* **1995**, *117*, 7245−7246.

(16) Smith, P. H.; Reyes, Z. E.; Lee, C. W.; Raymond, K. N. *Inorg. Chem.* **1988**, *27*, 4154−4165.

(17) Dietrich, B.; Viout, P.; Lehn, J.-M. *Macrocyclic Chemistry*; VCH: Weinheim, New York, Basel, and Cambridge, 1992.

(18) Koshland, D. A. *Angew. Chem., Int. Ed. Engl.* **1994**, *33*, 2375−2378.

(19) Burdinski, D.; Birkelbach, F.; Gerdan, M.; Trautwein, A. X.; Wieghardt, K.; Chandhuri, P. *J. Chem. Soc., Chem. Commun.* **1995**, 963−964.

(20) Goodman, M. S.; Hamilton, A. D.; Weiss, J. *J. Am. Chem. Soc.* **1995**, *117*, 8447−8455.

(21) Piguet, C.; Bünzli, J.-C. G.; Bernardinelli, G.; Bochet, C. G.; Froidevaux, P. *J. Chem. Soc., Dalton Trans.* **1995**, 83−97.

(22) Piguet, C.; Bernardinelli, G.; Bocquet, B.; Schaad, O.; Williams, A. F. *Inorg. Chem.* **1994**, *33*, 4112−4121.

(23) Piguet, C.; Rivara-Minten, E.; Hopfgartner, G.; Bünzli, J.-C. G. *Helv. Chim. Acta* **1995**, *78*, 1541−1566. Piguet, C.; Hopfgartner, G.; Williams, A. F.; Bünzli, J.-C. G. *J. Chem. Soc., Chem. Commun.* **1995**, 491−493.

(24) Piguet, C.; Rivara-Minten, E.; Hopfgartner, G.; Bünzli, J.-C. G. *Helv. Chim. Acta* **1995**, *78*, 1651−1672.

(25) Paul-Roth, C.; Raymond, K. N. *Inorg. Chem.* **1995**, *34*, 1408−1412. Amin, S.; Voss, D. A.; Horrocks, W. de W., Jr.; Lake, C. H.; Churchill, M. R.; Morrow, J. R. *Inorg. Chem.* **1995**, *34*, 3294−3300.

(26) (a) Sabbatini, N.; Guardigli, M.; Mecati, A.; Balzani, V.; Ungaro, R.; Ghildini, E.; Casnati, A.; Pochini, A. *J. Chem. Soc., Chem. Commun.* **1990**, 878−879; Hazenkamp, M. F.; Blasse, G.; Sabbatini, N.; Ungaro, R. *Inorg. Chim. Acta* **1991**, *172*, 93−95; (b) Brayshaw, P. A.; Bünzli, J.-C. G.; Froidevaux, P.; Harrowfield, J. M.; Kim, Y.; Sobolev, A. N. *Inorg. Chem.* **1995**, *34*, 2068−2076.

(27) Piguet, C.; Bernardinelli, G.; Bünzli, J.-C. G.; Petoud, S.; Hopfgartner, G. *J. Chem. Soc., Chem. Commun.* **1995**, 2575−2577.

(28) Black, G.; Depp, E.; Corson, B. B. *J. Org. Chem.* **1949**, *14*, 14−21.

Preparation of *N,N*-Diethyl-6-methylpyridine-2-carboxamide (2). 6-Methylpyridine-2-carboxylic acid (**1**; 20.0 g, 0.146 mol) was refluxed in freshly distilled thionyl chloride (100 mL, 1.37 mol) with dry DMF (500 μL) for 2 h. Excess thionyl chloride was evaporated and the crude residue coevaporated with 1,2-dichloroethane (50 mL). The solid residue was dried under vacuum and then dissolved in dichloromethane (200 mL), and dry *N,N*-diethylamine (53.4 g, 0.73 mol) was added dropwise under an inert atmosphere. The resulting solution was refluxed for 2 h and evaporated. The brown residue was partitioned between dichloromethane (200 mL) and half-saturated aqueous NH_4Cl solution (200 mL). The aqueous phase was extracted with dichloromethane (2 × 100 mL), the combined organic phase dried (Na_2SO_4) and evaporated, and the resulting brown oil distilled (83 °C, 10^{-2} Torr) to give 22.0 g (0.114 mol, yield 78%) of **2** as a colorless wax, mp 45−46 °C. ^{1}H NMR in $CDCl_3$: δ 1.14 (3H, t, $J^3 = 7$ Hz), 1.24 (3H, t, $J^3 = 7$ Hz), 2.53 (3H, s), 3.30 (2H, q, $J^3 = 7$ Hz), 3.52 (2H, q, $J^3 = 7$ Hz), 7.13 (1H, d, $J^3 = 8$ Hz), 7.29 (1H, t, $J^3 = 8$ Hz), 7.61 (1H, d, $J^3 = 8$ Hz). EI-MS: *m/z* 192 (M^+).

Preparation of 6-(*N,N*-Diethylcarbamoyl)pyridine-2-carboxylic Acid (3). *N,N*-Diethyl-6-methylpyridine-2-carboxamide (**2**; 21.5 g, 0.112 mol) and selenium dioxide (55.8 g, 0.503 mol) were refluxed in dry pyridine for 72 h under an inert atmosphere. After cooling, the mixture was filtered to remove solid Se and evaporated to dryness. The solid residue was suspended in water (700 mL) and the pH adjusted to 9.5 with NaOH (5 M). The resulting clear solution was extracted with dichloromethane (3 × 250 mL) and the aqueous phase filtered, acidified to pH 3.0 with hydrochloric acid (37%), concentrated, and cooled to −5 °C for 12 h. The resulting white crystals were collected by filtration and crystallized from hot acetonitrile to give 13.5 g (61 mmol, yield 55%) of **3**, mp 196−198 °C. ^{1}H NMR in CD_3OD: δ 1.18 (3H, t, $J^3 = 7$ Hz), 1.28 (3H, t, $J^3 = 7$ Hz), 3.32 (2H, q, $J^3 = 7$ Hz), 3.57 (2H, q, $J^3 = 7$ Hz), 4.91 (1H, s), 7.74 (1H, d.d, $J^3 = 8$ Hz, $J^4 = 1$ Hz), 8.09 (1H, t, $J^3 = 8$ Hz), 8.20 (1H, d.d, $J^3 = 8$ Hz, $J^4 = 1$ Hz). EI-MS: *m/z* 222 (M^+).

Preparation of 6-(*N,N*-Diethylcarbamoyl)-*N*-methyl-*N*-{4′-{4″-{*N*-methyl-*N*-[(5‴-methylpyridin-2‴-yl)carbonyl]amino}-3″-nitrobenzyl}-2′-nitrophenyl}pyridine-2-carboxamide (5). A mixture of **3** (1.19 g, 5.34 mmol), freshly distilled thionyl chloride (6.35 g, 53.0 mmol), and DMF (100 μL) was refluxed for 90 min in dry dichloromethane (50 mL). The mixture was evaporated and dried under vacuum and the solid residue dissolved in dichloromethane (100 mL) and added dropwise to a solution of *N*,5-dimethyl-*N*-{4′-[4″-(methylamino)-3″-nitrobenzyl]-2′-nitrophenyl}pyridine-2-carboxamide (**4**; 0.775 g, 1.78 mmol) and triethylamine (0.9 g, 8.9 mmol) in dichloromethane (50 mL). The solution was refluxed for 4 h under an inert atmosphere and the crude product isolated according to the standard workup procedure described for **2** and purified by column chromatography (Silicagel, CH_2Cl_2/MeOH, 99.2:0.8 → 98:2) to give 0.807 g (1.26 mmol, yield 71%) of **5** as a pale yellow solid, mp 90−93 °C dec. ^{1}H NMR in $CDCl_3$: δ 0.8−1.3 (6H, m), 2.2−2.4 (3H, m), 2.8−3.7 (4H, m), 3.50 (6H, s), 4.0−4.2 (2H, m), 7.1−8.5 (12H, m). ES-MS: *m/z* 640.2 ($[M + H]^+$). EI-MS: *m/z* 593 ($[M - NO_2]^+$).

Preparation of 2-{6-[*N,N*-Diethylcarbamoyl]pyridin-2-yl}-1,1′-dimethyl-5,5′-methylene-2′-(5-methylpyridin-2-yl)bis[1*H*-benzimidazole] (L^2). To a solution of **5** (0.807 g, 1.26 mmol) in ethanol/water (250 mL/64 mL), activated iron powder (2.11 g, 37.8 mmol), and concentrated hydrochloric acid (37%, 7.9 mL, 94.8 mmol) were added. The mixture was refluxed for 6 h under an inert atmosphere, the excess of iron was filtered off, and ethanol was distilled under vacuum. The resulting mixture was poured into dichloromethane (300 mL), $Na_2H_2EDTA \cdot 2H_2O$ (25 g) in water (150 mL) was added, and the resulting stirred mixture was neutralized (pH 7.0) with concentrated aqueous NH_4OH solution. Concentrated H_2O_2 solution (30%, 1 mL) was added under vigorous stirring, and the pH was adjusted to 8.5 with aqueous NH_4OH solution. After 15 min, the organic layer was separated and the aqueous phase extracted with dichloromethane (3 × 200 mL). The combined organic phases were dried (Na_2SO_4) and evaporated and the crude residue purified by column chromatography (Silicagel, CH_2Cl_2/MeOH 98.5:1.5 → 97:3) and then crystallized from hot acetonitrile to give 0.537 g (0.988 mmol, yield 78%) of ligand L^2 as colorless plates, mp 69−71 °C. ^{1}H NMR in $CDCl_3$: δ 1.13 (3H, t, $J^3 = 7$ Hz), 1.30 (3H, t, $J^3 = 7$ Hz), 2.42 (3H, s), 3.35 (2H, q, $J^3 = 7$ Hz), 3.61 (2H, q, $J^3 = 7$ Hz), 4.21 (3H, s), 4.24 (3H, s), 4.29 (2H, s), 7.20 (1H, d.d, $J^3 = 8$ Hz, $J^4 = 1$ Hz), 7.23 (1H, d.d, $J^3 = 8$ Hz, $J^4 = 1$ Hz), 7.33 (1H, d, $J^3 = 8$ Hz), 7.34 (1H, d, $J^3 = 8$ Hz), 7.57 (1H, d, $J^3 = 8$ Hz), 7.69 (1H, d, $J^4 = 1$ Hz), 7.71 (1H, d, $J^4 = 1$ Hz), 7.93 (1H, t, $J^3 = 8$ Hz), 8.20 (1H, d, $J^3 = 8$ Hz), 8.38 (1H, m), 8.51 (1H, m). ^{13}C NMR in $CDCl_3$: δ 12.79, 14.29, 18.42, 32.62 (primary C); 39.74, 42.20, 42.94 (secondary C); 109.69, 109.81, 119.72, 119.89, 122.59, 124.14, 124.44, 125.00, 125.62, 137.28, 137.83, 148.89 (tertiary C); 133.41, 135.80, 136.16, 136.65, 142.77, 142.79, 148.02, 149.35, 149.73, 150.54, 154.18, 168.36 (quaternary C). EI-MS: *m/z* 543 (M^+). X-ray quality colorless prisms of L^2 were obtained by slow cooling (6 days) of a hot concentrated acetonitrile solution.

Preparation of the Complexes. The perchlorate salts $Ln(ClO_4)_3 \cdot nH_2O$ (Ln = La, Pr, Nd, Sm, Eu, Tb, Tm, Yb, Lu, Y; n = 6−8) were prepared from the corresponding oxides (Glucydur, 99.99%) according to a literature method.[30] $Ce(ClO_4)_3 \cdot 5.8H_2O$ was obtained by metathesis of cerium(III) carbonate hydrate (Aldrich, 99.9%) with aqueous perchloric acid.

Preparation of $[Zn_2(L^2)_2](ClO_4)_4$ (7). L^2 (54.4 mg, 0.1 mmol) in 1:1 dichloromethane/acetonitrile (4 mL) was slowly added to $Zn(ClO_4)_2 \cdot 6H_2O$ (37.2 mg, 0.1 mmol) in acetonitrile (5 mL). The resulting solution was evaporated, the solid residue dissolved in acetonitrile (3 mL), and diethyl ether slowly diffused into the solution for 2 days. White microcrystals were separated by filtration to give 59 mg (36.5 μmol, yield 73%) of hygroscopic $[Zn_2(L^2)_2](ClO_4)_4$ (**7**).

Preparation of $[LnZn(L^2)_3](ClO_4)_5 \cdot 0.5C_4H_{10}O \cdot 2H_2O$ (Ln = La, 8; Nd, 9; Eu, 10; Gd, 11; Tb, 12). A solution of 61.3 μmol of $Ln(ClO_4)_3 \cdot nH_2O$ (Ln = La, Nd, Eu, Gd, Tb) and 22.8 mg (61.3 μmol) of $Zn(ClO_4)_2 \cdot 6H_2O$ in acetonitrile (5 mL) was slowly added to a solution of L^2 (0.1 g, 0.184 mmol) in 1:1 dichloromethane/acetonitrile (10 mL). After being stirred at room temperature for 1 h, the solution was evaporated, the solid residue dissolved in acetonitrile (4 mL), and diethyl ether diffused into the solution for 2−3 days. The resulting white microcrystalline aggregates were collected by filtration and dried to give 84−92% of complexes $[LnZn(L^2)_3](ClO_4)_5 \cdot 0.5Et_2O \cdot 2H_2O$ (Ln = La, **8**; Nd, **9**; Eu, **10**; Gd, **11**; Tb, **12**). X-ray quality crystals of $[EuZn(L^2)_3](ClO_4)(CF_3SO_3)_4(CH_3CN)_4$ (**13**) were obtained by slow diffusion of diisopropyl ether into an acetonitrile solution of **10** containing 30 equiv of $NBu_4CF_3SO_3$. After 5 days, the resulting two separated liquid phases were mixed using an ultrasonic bath to give a white emulsion which gave fragile colorless prisms of **13** upon slow cooling at 277 K. Complexes **7**−**12** were characterized by their IR spectra and give satisfactory elemental analyses (Table SII in the supporting information).

For the purpose of the photophysical study, europium-doped La (**8a**) and Gd (**11a**) complexes were prepared by replacing the lanthanide solution by an Eu (2%)/Ln (98%) mixed solution.

Preparation of $[LnZn(L^2)_3](ClO_4)_5$ (Ln = Ce, 14; Pr, 15; Sm, 16; Tm, 17; Yb, 18; Lu, 19; Y, 20). These complexes were prepared *in situ* for ^{1}H NMR studies. A 263 μL (5.26 μmol) portion of an equimolar 10^{-2} M solution of $Ln(ClO_4)_3 \cdot nH_2O$ (Ln = Ce, Pr, Sm, Tm, Yb, Lu, Y) and $Zn(ClO_4)_2 \cdot 6H_2O$ in acetonitrile was added to L^2 (8.6 mg, 15.8 μmol), dissolved in 4 mL of 1:1 dichloromethane/acetonitrile. After evaporation of the solution, the solid residue was dried under vacuum and then dissolved in 700 μL of degassed CD_3CN to give a 7.5 mM solution of $[LnZn(L^2)_3](ClO_4)_5$ (Ln = Ce, **14**; Pr, **15**; Sm, **16**; Tm, **17**; Yb, **18**; Lu, **19**; Y, **20**) which was used without further purification. ***Caution!*** Perchlorate salts combined with organic ligands are potentially explosive and should be handled with the necessary precautions.[31]

Physicochemical Measurements. Reflectance spectra were recorded as finely grounded powders dispersed in MgO (5%) with MgO as the reference on a Perkin-Elmer Lambda 19 spectrophotometer equipped with a Labsphere RSA-PE-19 integration sphere. Electronic spectra in the UV−vis range were recorded at 20 °C from 10^{-3} M acetonitrile solutions with Perkin-Elmer Lambda 5 and Lambda 7

(29) Piguet, C.; Bocquet, B.; Hopfgartner, G. *Helv. Chim. Acta* **1994**, *77*, 931−942.

(30) Desreux, J. F. In *Lanthanide Probes in Life, Chemical and Earth Sciences*, Bünzli, J.-C. G., Choppin, G. R., Eds.; Elsevier Publishing Co.: Amsterdam, 1989; Chapter 2, p 43.

(31) Wolsey, W. C. *J. Chem. Educ.* **1978**, *55*, A355.

spectrometers using quartz cells of 0.1 and 0.01 cm path length. Spectrophotometric titrations were performed with a Perkin-Elmer Lambda 5 spectrophotometer connected to an external computer. In a typical experiment, 50 mL of ligand (L^2) in acetonitrile (10^{-4} M) was titrated at 20 °C with an equimolar solution of $Ln(ClO_4)_3 \cdot nH_2O$ and $Zn(ClO_4)_2 \cdot 6H_2O$ (0.83 mM) in acetonitrile. After each addition of 0.20 mL, the absorbances at 10 different wavelengths were recorded using a 0.1 cm quartz cell and transferred to the computer. Plots of extinction as a function of the metal:ligand ratio gave a first indication of the number and stoichiometry of the complexes formed; factor analysis[32] was then applied to the data to confirm the number of different absorbing species. Finally, a model for the distribution of species was fitted with a nonlinear least-squares algorithm to give stability constants as previously described.[33] IR spectra were obtained from KBr pellets with a Perkin-Elmer 883 spectrometer. ^{1}H, ^{13}C, and ^{113}Cd NMR spectra were recorded at 25 °C on a broad band Varian Gemini 300 spectrometer. Chemical shifts are given in parts per million with respect to TMS. EI-MS (70 eV) spectra were recorded with VG-7000E and Finnigan-4000 instruments. Pneumatically-assisted electrospray (ES-MS) mass spectra were recorded from 10^{-4} M acetonitrile solutions on an API III tandem mass spectrometer (PE Sciex) by infusion at 4−10 μL/min. The spectra were recorded under low up-front declustering or collision-induced dissociation (CID) conditions, typically ΔV = 0−30 V between the orifice and the first quadrupole of the spectrometer.[34] Determination of the total charge (z) of the complexes was made by using the isotopic pattern ($z \leq 3$) or adduct ions with perchlorate anions ($z > 3$).[35] The experimental procedures for high-resolution, laser-excited luminescence measurements have been published previously.[36] Solid state samples were finely powdered, and low temperature (77 or 10 K) was achieved by means of a Cryodyne Model 22 closed-cycle refrigerator from CTI Cryogenics. Luminescence spectra were corrected for the instrumental function, but not excitation spectra. Lifetimes are averages of at least 3−5 independent determinations. Quantum yields, ligand excitation, and emission spectra were recorded on a Perkin-Elmer LS-50 spectrometer equipped for low-temperature measurements. The relative quantum yields were calculated using the following formula:[21] $Q_x/Q_r = \langle A_r(\lambda_r)/A_x(\lambda_x)\rangle\langle I(\lambda_r)/I(\lambda_x)\rangle\langle n_x^2/n_r^2\rangle\langle D_x/D_r\rangle$ where the subscript r stands for the reference and x for the samples, A is the absorbance at the excitation wavelength, I is the intensity of the excitation light at the same wavelength, n is the refractive index (1.341 for all solutions in acetonitrile), and D is the measured integrated luminescence intensity.

Crystal Structure Determination of L^2. Crystal data for $C_{33}H_{33}N_7O$: M = 543.7, monoclinic, $P2_1/c$, a = 17.7172(7) Å, b = 7.4444(3) Å, c = 21.229(1) Å, β = 98.545(5)°, U = 2768.9(2) Å^3 (by least-squares refinement of 25 reflections, 44° ≤ 2θ ≤ 55°), Z = 4, D_c = 1.30 g·cm^{-3}, $F(000)$ = 1152, colorless prisms, crystal dimensions 0.10 × 0.26 × 0.33 mm, μ(Cu Kα) = 0.651 mm^{-1}. Data collection and processing: Nonius CAD4 diffractometer, T = 170 K, ω−2θ scan, scan width 1.5 + 0.14 tan θ, scan speed 0.09 deg·s^{-1}, Cu Kα radiation (λ = 1.5418 Å); 3554 reflections measured (4 ≤ 2θ ≤ 110°, −18 < h < 18, 0 < k < 7, 0 < l < 22), 3452 unique reflections (R_{int} for equivalent reflections 0.024) of which 2886 were observable ($|F_o| > 4\sigma(F_o)$). Two reference reflections were measured every 30 min and showed a variation in intensity of <2.8 $\sigma(I)$. *Structure analysis and refinement:* Data were corrected for Lorentz, polarization, and absorption effects[37] (A^*_{min} = 1.066, A^*_{max} = 1.186). The structure was solved by direct methods using MULTAN 87;[38] all other calculations used the XTAL[39] system and ORTEP II[40] programs. Full-matrix least-squares refinements (on F) using weights of $w = 1/\sigma^2(F_o)$ gave final values of R = 0.045 and R_w = 0.034 for 470 variables and 2886 contributing reflections. The mean shift/error on the last cycle was 0.81 × 10^{-2}, and the maximum was 0.25. H atoms were observed and refined with fixed isotropic displacement parameters (U = 0.05 Å^2), and the 41 non-hydrogen atoms were refined with anisotropic displacement parameters. The final Fourier difference synthesis showed a maximum of +0.29 and a minimum of −0.33 e Å^{-3}.

Crystal Structure Determination of $[EuZn(L^2)_3](ClO_4)(CF_3SO_3)_4(CH_3CN)_4$ (13). Crystal data for $EuZnC_{111}H_{111}N_{25}O_{19}F_{12}S_4Cl$: M = 2708.1, monoclinic, $C2/c$, a = 50.417(8) Å, b = 20.822(4) Å, c = 23.498(5) Å, β = 92.67(1)°, U = 24641(8) Å^3 (by least-squares refinement of 29 reflections, 38° ≤ 2θ ≤ 60°), Z = 8, D_c = 1.46 g·cm^{-3}, $F(000)$ = 11088, colorless prisms, crystal dimensions 0.10 × 0.25 × 0.28 mm, μ(Cu Kα) = 5.472 mm^{-1}. Data collection and processing: Nonius CAD4 diffractometer, T = 200 K, ω−2θ scan, scan width 1.5 + 0.14 tan θ, scan speed 0.137 deg·s^{-1}, Cu Kα radiation (λ = 1.5418 Å); 13 029 reflections measured (4 ≤ 2θ ≤ 100°, −50 < h < 50, 0 < k < 20, 0 < l < 23), 12 641 unique reflections (R_{int} for equivalent reflections 0.102) of which 7796 were observable ($|F_o| > 4\sigma(F_o)$). Two reference reflections were measured every 30 min and showed a total decrease in intensity of 5.4%. All intensities were corrected for this drift. Structure analysis and refinement: Data were corrected for Lorentz, polarization, and absorption effects[37] (A^*_{min} = 1.725, A^*_{max} = 4.387). The structure was solved by direct methods as described for L^2. Full-matrix least-squares refinements (on F) gave final values of $R = R_w$ = 0.102 (w = 1) for 1520 variables and 7796 contributing reflections. The non-H atoms of the solvent molecules were refined with isotropic displacement parameters (12 atoms) and all the other atoms (180) with anisotropic displacement parameters. The perchlorate, the triflate anion g, and the acetonitrile molecules are disordered and were refined with restraints on bond distances and angles. H atoms were placed in calculated positions and contributed to F_c calculations. The final Fourier difference synthesis showed a maximum of +1.61 and a minimum of −2.08 e Å^{-3} located around the Eu atom.

Results

Preparation of the Ligand L^2. The segmental ligand 2-{6-[*N*,*N*-diethylcarbamoyl]pyridin-2-yl}-1,1′-dimethyl-5,5′-methylene-2′-(5-methylpyridin-2-yl)bis[1*H*-benzimidazole] (L^2) is obtained in two steps from the synthons **3** and **4** according to a strategy based on a modified Phillips-type coupling reaction as the key step for the synthesis of benzimidazole rings from *N*-(2-nitroaryl)arenecarboxamide precursors (Scheme 1).[29] The asymmetric synthon **3** is obtained in good yield from 6-methylpyridine-2-carboxylic acid (**1**) using a usual amidation procedure[29] followed by the oxidation of the methyl group bound to the 6-position of the pyridine ring with anhydrous selenium dioxide in pyridine.[41] This new approach was preferred to the reported direct reaction of pyridine-2,6-dicarboxylic acid with a stoichiometric amount of trifluoroacetic anhydride followed by treatment with amines which gives only moderate yield of asymmetric amides together with significant quantities of unreacted starting materials and diamide byproducts.[42] **3** is transformed into the acyl chloride with thionyl chloride[29] and then reacted with **4**[29] to give the asymmetric *o*-dinitro dicarboxamide compound **5**. The key step, the reduction of **5** by Fe, could lead to two possible isomers: the target ligand L^2 and **6** resulting from the cyclization of the two carboxamide groups attached to the 2- and 6-positions of the same pyridine ring. TLC shows that only one isomer is formed, but NMR,

(32) Malinowski, E. R.; Howery, D. G. *Factor Analysis in Chemistry*, J. Wiley: New York, Chichester, Brisbane, and Toronto, 1980.
(33) Piguet, C.; Bernardinelli, G.; Bocquet, B.; Quattropani, A.; Williams, A. F. *J. Am. Chem. Soc.* **1992**, *114*, 7440−7451.
(34) Hopfgartner, G.; Piguet, C.; Henion, J. D.; Williams, A. F. *Helv. Chim. Acta* **1993**, *76*, 1759−1766.
(35) Hopfgartner, G.; Piguet, C.; Henion, J. D. *J. Am. Soc. Mass Spectrom.* **1994**, *5*, 748−756.
(36) Piguet, C.; Williams, A. F.; Bernardinelli, G.; Moret, E.; Bünzli, J.-C. G. *Helv. Chim. Acta* **1992**, *75*, 1697−1717.
(37) Blanc, E.; Schwarzenbach, D.; Flack, H. D. *J. Appl. Crystallogr.* **1991**, *24*, 1035−1041.
(38) Main, P.; Fiske, S. J.; Hull, S. E.; Lessinger, L.; Germain, D.; Declercq, J. P.; Woolfson, M. M. *MULTAN 87*; Universities of York, England, and Louvain-La-Neuve, Belgium, 1987.
(39) Hall, S. R., Stewart, J. M., Eds. *XTAL 3.2 User's Manual*; Universities of Western Australia and Maryland, 1992.
(40) Johnson, C. K. ORTEP II; Report ORNL-5138; Oak Ridge National Laboratory: Oak Ridge, TN, 1976.
(41) Piguet, C.; Bünzli, J.-C. G.; Bernardinelli, G.; Hopfgartner, G.; Williams, A. F. *J. Am. Chem. Soc.* **1993**, *115*, 8197−8206.
(42) Reddy, K. V.; Jin, S.-J.; Arora, P. K.; Sfeir, D. S.; Maloney, S. C. F.; Urbach, F. L.; Sayre, L. M. *J. Am. Chem. Soc.* **1990**, *112*, 2332−2340.

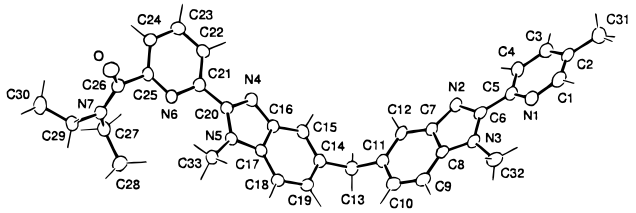

Figure 1. Numbering scheme and ORTEP[40] view of L^2 with ellipsoids represented at 50% probability level.

Scheme 1

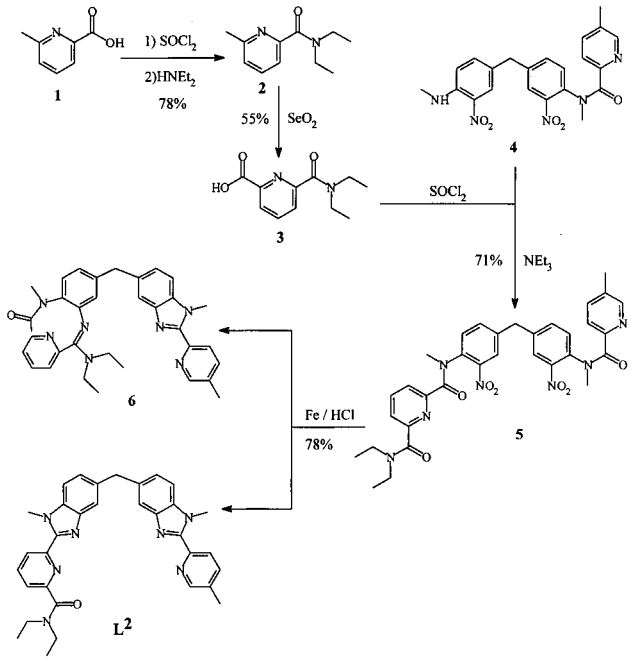

IR, and MS data do not allow the two possible isomers to be clearly distinguished, even though we expect severe steric constraints for the nine-membered ring in **6**.[43] The X-ray crystal structure definitely establishes that L^2 is the only isomer formed (Figure 1) and shows that the pyridine and the benzimidazole rings within each coordinating unit adopt a transoid conformation (s-trans, i.e., N(1) trans to N(2) and N(4) trans to N(6); dihedral angles between pyridine and benzimidazole least-squares planes 14.0(1)° (bidentate unit) and 17.4(1)° (tridentate unit)). The carboxamide group (C(25)−C(26)−O−N(7)) is planar within experimental error and adopts a distorted transoid conformation (O trans to N(6), dihedral angle between the least-squares planes of the pyridine (N(6)) and the carboxamide group 49.8(1)°). All bond lengths and angles within the ligand are typical[44] and are given in the supporting information. As often observed with polyaromatic heterocyclic ligands,[45] intermolecular π-stacking interactions occur between parallel bidentate coordinating units (average distance between aromatic planes 3.6 Å), leading to closely packed pairs of ligands in the solid state. Detailed NOEDIF measurements of L^2 in chloroform show significant nuclear Overhauser effects (NOE) between Me^2 and H^1, but no effects are detected between Me^2 and H^3 and Me^3 and H^{12}, strongly suggesting that the pyridine and benzimidazole rings adopt similar transoid arrangement in solution which is crucial for the coordination behavior of L^2 since the transoid → cisoid conformational change associated with lanthanide complexation controls the stability and the selectivity of the final complexes.[21,46]

Following the Assembly Processes of L^2 with d- and f-Block Metal Ions. The ligand L^2 possesses two different binding units connected by a methylene spacer which favors the formation of polynuclear complexes.[33,41,47] The bidentate unit is coded for the coordination of pseudooctahedral d-block metal ions[22] while the tridentate unit is suitable for the pseudotricapped trigonal prismatic coordination of Ln(III).[27] We thus expect the binding units of L^2 to simultaneously recognize 3d and 4f metal ions, leading to the selective formation of heterodinuclear d−f complexes. Our strategy is based on the following approach: (i) study of the homopolynuclear complexes formed by L^2 with Zn(II) and La(III), (ii) detailed characterization of the assembly processes leading to the heteronuclear d−f complexes, and (iii) structural characterization of the latter both in the solid state and in solution. In order to limit the amount of ligand required for the studies, we have resorted to electrospray mass spectrometry (ES-MS) for the qualitative speciation,[34,35] spectrophotometric titrations for the quantitative analysis of the assembly processes,[47] and ^{1}H NMR and luminescence techniques for the structural investigations,[23] using Ln(III) as the shift reagent[48] and luminescent probe.[1] The complexes were isolated as their perchlorate salts to avoid any anion coordination.

Homonuclear Complexes of L^2 with La(III). Upon complexation to metal ions, the electronic $\pi \rightarrow \pi^*$ transitions centered on ligand L^2 (maximum of the band envelope at 33 320 cm^{-1}) are shifted toward lower energies, allowing the monitoring of the complex formation. Titrations of L^2 with $La(ClO_4)_3 \cdot nH_2O$ in acetonitrile have been performed for total ligand concentrations of $10^{-4}-10^{-5}$ M and La:L^2 ratios in the range 0.1−1.8. Complicated variations of the UV absorbances (Figure 2a) and factor analysis[32] suggest the existence of at least four absorbing complexes. The spectrophotometric data can be fitted to equilibria 1−4 where convergence is observed with a root-mean-

$$La^{3+} + 3L^2 \leftrightarrow [La(L^2)_3]^{3+} \quad \log(\beta_{13}^{La}) = 19.6(5) \quad (1)$$

$$2La^{3+} + 3L^2 \leftrightarrow [La_2(L^2)_3]^{6+} \quad \log(\beta_{23}^{La}) = 27.5(9) \quad (2)$$

$$2La^{3+} + 2L^2 \leftrightarrow [La_2(L^2)_2]^{6+} \quad \log(\beta_{22}^{La}) = 22.3(9) \quad (3)$$

$$3La^{3+} + 2L^2 \leftrightarrow [La_3(L^2)_2]^{9+} \quad \log(\beta_{32}^{La}) = 29.0(9) \quad (4)$$

square (RMS) difference between calculated and observed absorbances of 0.001 unit or less. However, the great similarity between the reconstructed spectra of the four complexes prevents an accurate determination of the stability constants which are thus only mere estimations.

Unfortunately, homonuclear complexes of segmental ligands with Ln(III) are known to give a weak ES-MS response[23,24] as a result of the poor matching between the ligand binding

(43) March, J. *Advanced Organic Chemistry*, 4th ed.; J. Wiley & Sons: New York, Chichester, Brisbane, Toronto, and Singapore, 1992; pp 155−161.

(44) Allen, F. H.; Kennard, O.; Watson, D. G.; Brammer, L.; Orpen, A. G.; Taylor, R. *J. Chem. Soc., Perkin Trans. 2*, **1987**, S1−S19.

(45) Chisholm, M. H.; Huffman, J. C.; Rothwell, I. P.; Bradley, P. G.; Kress, N.; Woodruff, W. H. *J. Am. Chem. Soc.* **1981**, *103*, 4945−4947. Constable, E. C.; Elder, S. M.; Healy, J. A.; Tocher, D. A. *J. Chem. Soc., Dalton Trans.* **1990**, 1669−1674. Constable, E. C.; Elder, S. M.; Walker, J. V.; Wood, P. P.; Tocher, D. A. *J. Chem. Soc., Chem. Commun.* **1992**, 229−231. Constable, E. C.; Cargill-Thompson, A. M. W.; Harveson, P.; Macko, L.; Zehnder, M. *Chem. Eur. J.* **1995**, *1*, 360−367.

(46) Piguet, C.; Bünzli, J.-C. G.; Bernardinelli, G.; Williams, A. F. *Inorg. Chem.* **1993**, *32*, 4139−4149.

(47) Piguet, C.; Hopfgartner, G.; Bocquet, B.; Schaad, O.; Williams, A. F. *J. Am. Chem. Soc.* **1994**, *116*, 9092−9102.

(48) Bertini, I.; Luchinat, C. *NMR of Paramagnetic Molecules in Biological Systems*; Benjamin/Cummings Publishing Co.: Menlo Park, CA, 1986; Chapter 10. Bertini, I.; Turano, P.; Vila, A. J. *Chem. Rev.* **1993**, *93*, 2833−2932.

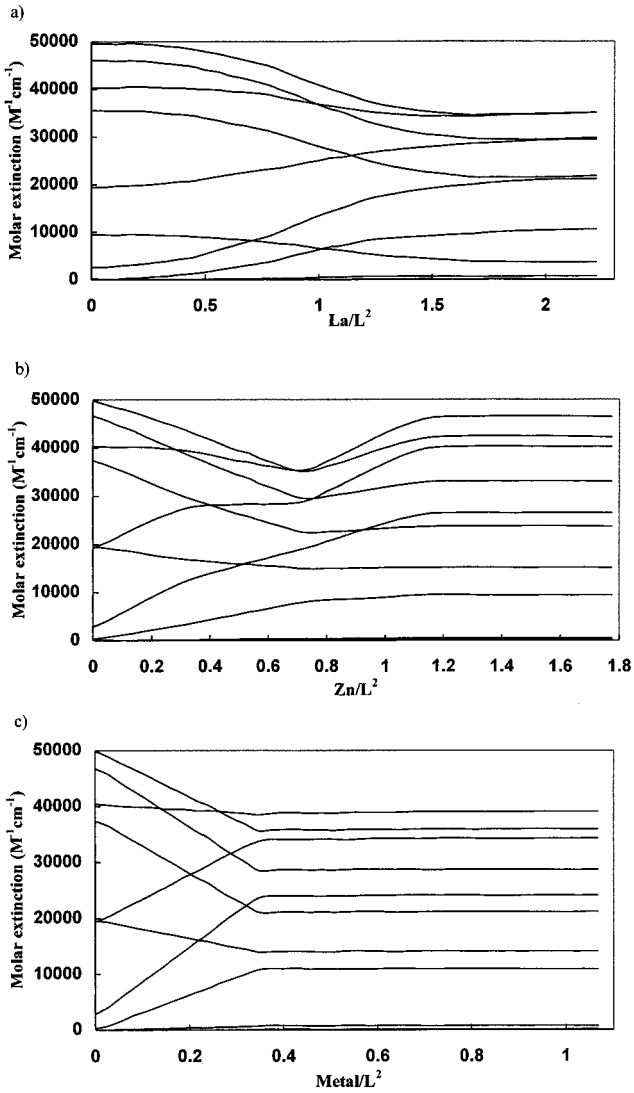

Figure 2. Variation of observed molar extinctions at 10 different wavelengths for the spectrophotometric titrations of L^2 with (a) $La(ClO_4)_3 \cdot 6H_2O$, (b) $Zn(ClO_4)_2 \cdot 6H_2O$, and (c) an equimolar mixture of $La(ClO_4)_3 \cdot 6H_2O$ and $Zn(ClO_4)_2 \cdot 6H_2O$ (metal concentration = La(III) concentration = Zn(II) concentration) in CH_3CN at 293 K (total ligand concentration 10^{-4} M).

possibilities and the large coordination numbers required by Ln(III),[41] which lead to solvated species difficult to transfer into the gaseous phase.[23,35] Titrations of L^2 with La(III) show only significant peaks for the free ligand (*m*/*z* 544.2 and 1087.6 corresponding to $[L^2 + H]^+$ and $[2L^2 + H]^+$, respectively), and we were unable to confirm the speciation established by spectrophotometry. ^{1}H NMR titrations of L^2 with $La(ClO_4)_3 \cdot 6H_2O$ in CD_3CN lead to intricate mixtures of low-symmetry complexes displaying slow chemical exchange processes on the NMR time scale. This behavior strongly contrasts with the selective and quantitative formation of the head-to-tail C_1-triple helicate $[La_2(L^1)_3]^{6+}$ under similar conditions.[23] The complexes between L^2 and La(III) were not further investigated.

Homonuclear Complexes of L^2 with Zn(II). ES-MS titrations of L^2 with $Zn(ClO_4)_2 \cdot 6H_2O$ in acetonitrile for Zn:L^2 ratios in the range 0.1−2.0 show the formation of four successive complexes, $[Zn(L^2)_3]^{2+}$ (*m*/*z* 847.8), $[Zn(L^2)_2]^{2+}$ (*m*/*z* 576.4), $[Zn_2(L^2)_3]^{4+}$ (*m*/*z* 440.4), and $[Zn_2(L^2)_2]^{4+}$ (*m*/*z* 304.8), and their adducts[35] with perchlorate anions (Table 1). The systematic observation of many different complexes for each Zn:L^2 ratio suggests the formation of intricate mixtures in solution. Spectrophotometric data obtained in the same conditions display three end points for Zn:L^2 ratios of 0.3, 0.6, and 1.1 (Table 2, Figure 2b). Factor analysis[32] points to three absorbing complexes, and the data can be fitted to equilibria 5−7 (RMS = 0.003). We were unable to satisfactorily

$$Zn^{2+} + 3L^2 \leftrightarrow [Zn(L^2)_3]^{2+} \quad \log(\beta_{13}^{Zn}) = 22(1) \quad (5)$$

$$2Zn^{2+} + 3L^2 \leftrightarrow [Zn_2(L^2)_3]^{4+} \quad \log(\beta_{23}^{Zn}) = 28.4(8) \quad (6)$$

$$2Zn^{2+} + 2L^2 \leftrightarrow [Zn_2(L^2)_2]^{4+} \quad \log(\beta_{22}^{Zn}) = 21.5(9) \quad (7)$$

reproduce the data with a model including the species $[Zn(L^2)_2]^{2+}$ observed by ES-MS, probably as a result of too similar absorption spectra for the different complexes, which strongly suggests that the reported stability constants are only estimations.[47]

Upon complexation to Zn(II), the ^{1}H NMR spectrum of L^2 is broadened by slow chemical exchanges on the NMR time scale and is of no use for the structural characterization of the homonuclear complexes. We observe a sharp end point for Zn:L^2 = 1.0 and the formation of >90% (from integration of the NMR signals) of the complex $[Zn_2(L^2)_2]^{4+}$ which displays 23 well-resolved ^{1}H NMR signals fully assigned by using COSY, NOESY, and NOEDIF techniques (Table 3). This feature corresponds to two equivalent ligands L^2 coordinated to Zn(II) and related by a C_2 axis. The presence of the diastereotopic methylene protons $H^{7,8}$, $H^{15,16}$, and $H^{17,18}$ and the observation of 33 signals in the ^{13}C NMR spectrum preclude the existence of mirror planes[49] and point to C_2 symmetry for the complex $[Zn_2(L^2)_2]^{4+}$ in solution. NOEs between Me^2 and H^3, Me^3 and H^{12}, and $H^{17,18}$ and H^{14} show that the bidentate and the tridentate

Table 1. Molecular Peaks of Complexes of L^2 and Adduct Ions Observed by ES-MS

metal	cation	*m*/*z*[a]	metal	cation	*m*/*z*[a]
Zn(II)	$[Zn(L^2)_3]^{2+}$	847.8	Eu(III)/Zn(II)	$[EuZn(L^2)_3]^{5+}$	369.6
	$[Zn(L^2)_3(ClO_4)]^+$	1795.8		$[EuZn(L^2)_3(ClO_4)]^{4+}$	487.0
	$[Zn(L^2)_2]^{2+}$	575.8		$[EuZn(L^2)_3(ClO_4)_2]^{3+}$	682.2
	$[Zn(L^2)_2(ClO_4)]^+$	1251.6		$[EuZn(L^2)_3(ClO_4)_3]^{2+}$	1073.2
	$[Zn_2(L^2)_3]^{4+}$	440.4	Gd(III)/Zn(II)	$[GdZn(L^2)_3]^{5+}$	370.8
	$[Zn_2(L^2)_3(ClO_4)]^{3+}$	620.4		$[GdZn(L^2)_3(ClO_4)]^{4+}$	488.2
	$[Zn_2(L^2)_3(ClO_4)_2]^{2+}$	980.4		$[GdZn(L^2)_3(ClO_4)_2]^{3+}$	684.0
	$[Zn_2(L^2)_2]^{4+}$	304.8		$[GdZn(L^2)_3(ClO_4)_3]^{2+}$	1075.8
	$[Zn_2(L^2)_2(ClO_4)]^{3+}$	439.2	Tb(III)/Zn(II)	$[TbZn(L^2)_3]^{5+}$	371.0
	$[Zn_2(L^2)_2(ClO_4)_2]^{2+}$	709.4		$[TbZn(L^2)_3(ClO_4)]^{4+}$	488.3
La(III)/Zn(II)	$[LaZn(L^2)_3]^{5+}$	366.8		$[TbZn(L^2)_3(ClO_4)_2]^{3+}$	684.6
	$[LaZn(L^2)_3(ClO_4)]^{4+}$	483.4		$[TbZn(L^2)_3(ClO_4)_3]^{2+}$	1076.6
	$[LaZn(L^2)_3(ClO_4)_2]^{3+}$	678.1			
	$[LaZn(L^2)_3(ClO_4)_3]^{2+}$	1066.8			

[a] *m*/*z* values given for the maximum of the peak.

Table 2. Electronic Spectral Data for the Ligand L^2 and Its Heterodinuclear Complexes in Acetonitrile at 293 K[a]

compd	$\pi \rightarrow \pi^*$	compd	$\pi \rightarrow \pi^*$
L^2	33 320 (50 690)	$[GdZn(L^2)_3]^{5+}$	32 050 (101 500)
	31 750 (39 090 sh)		30 490 (82 260 sh)
$[LaZn(L^2)_3]^{5+}$	32 050 (101 330)	$[TbZn(L^2)_3]^{5+}$	32 050 (101 940)
	30 490 (79 660 sh)		30 490 (82 300 sh)
$[CeZn(L^2)_3]^{5+}$	32 050 (101 900)	$[TmZn(L^2)_3]^{5+}$	32 050 (102 840)
	30 490 (80 990 sh)		30 490 (86 230 sh)
$[PrZn(L^2)_3]^{5+}$	32 050 (102 600)	$[YbZn(L^2)_3]^{5+}$	32 050 (101 300)
	30 490 (82 790 sh)		30 490 (81 425 sh)
$[NdZn(L^2)_3]^{5+}$	32 050 (101 440)	$[LuZn(L^2)_3]^{5+}$	32 050 (101 950)
	30 490 (80 630 sh)		30 490 (85 500 sh)
$[SmZn(L^2)_3]^{5+}$	32 050 (101 640)	$[YZn(L^2)_3]^{5+}$	32 050 (101 870)
	30 490 (83 560 sh)		30 490 (84 320 sh)
$[EuZn(L^2)_3]^{5+}$	32 050 (102 050)		
	30 490 (81 880 sh)		

[a] Energies are given for the maximum of the band envelope in cm^{-1} and ϵ (in parentheses) in $M^{-1}\cdot cm^{-1}$; sh = shoulder.

binding units adopt cisoid conformations consecutive to their coordination to Zn(II). Further structural information is obtained from the intrastrand NOEs experienced by the proton of the methylene spacer.[23,47] The NOE map (H^6-H^9, H^7-H^9, H^7-H^{10}, H^8-H^5, H^8-H^6) is typical of a helical twist of L^2 which puts H^9 above the plane of the second benzimidazole ring connected to the methylene spacer, leading to a significant shielding effect for this proton ($\Delta\delta = 1.63$ ppm) as similarly reported for the double helicate $[Zn_2(L^1)_2]^{4+}$ ($\Delta\delta = 1.82$ ppm).[23] These observations imply a comparable double-helical structure for $[Zn_2(L^2)_2]^{4+}$ and exclude the side-by-side structures **III** and **IV** (Figure 3).[47] However, the two remaining possible helical structures **I** and **II** belong to the same C_2 point group and yield ^1H NMR spectra with very similar patterns. A weak interstrand NOE observed between H^1 and $H^{15,16}$ strongly suggests a head-to-tail arrangement of the ligands in $[Zn_2(L^2)_2]^{4+}$ which brings the terminal pyridine ring of one ligand close to the carboxamide

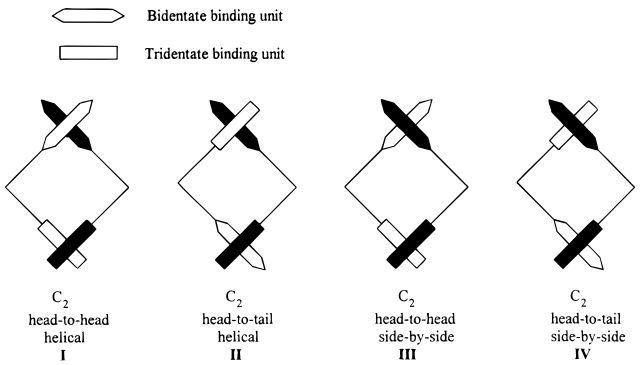

Figure 3. Possible structures for the complex $[Zn_2(L^2)_2]^{4+}$.

group of the second ligand (structure **II**), as reported for $[Pd_2(quinquepyridine)_2]^{4+}$.[50] Unfortunately, we were unable to record dependable ^{67}Zn NMR signals to confirm this hypothesis because the quadrupolar ^{67}Zn nucleus ($I = 5/2$)[48] induces very broad lines for poorly symmetrical polyaza complexes.[51] The replacement of Zn(II) by Cd(II) leads to a very similar behavior in solution: (i) $[Cd_2(L^2)_2]^{4+}$ (m/z 328.6) and its adduct ions[35] $[Cd_2(L^2)_2(ClO_4)_i]^{(4-i)+}$ (m/z 470.4, 756.2, and 1609.4 for $i = 1-3$, respectively) are observed in the ES-MS spectra, (ii) the ^1H NMR spectra are comparable (Table 3), and (iii) interstrand NOE occurs between H^1 and Me^4. The ^{113}Cd NMR spectrum of $[Cd_2(L^2)_2]^{4+}$ in acetonitrile displays only one singlet (δ 241.7 ppm with respect to $Cd(ClO_4)_2$ (0.1 M) in D_2O) which is typical of Cd(II) coordinated by four heterocyclic nitrogen atoms and one oxygen atom[52] and definitely establishes the helical head-to-tail structure **II** for $[Cd_2(L^2)_2]^{4+}$. In view of the comparable data for the Cd and Zn complexes, we infer that $[Zn_2(L^2)_2]^{4+}$ adopts structure **II** in solution, in contrast with the head-to-head helical structure **I** found for the analogous complex [Zn_2-

Table 3. ^1H NMR Shifts (with Respect to TMS) for Ligand L^2 in $CDCl_3$ and Its Complexes in CD_3CN at 298 K

Bidentate Binding Unit

compd	Me^1	Me^2	H^1	H^2	H^3	H^4	H^5	H^6	$H^{7,8}$
L^2	2.42	4.23	8.51	7.64	8.26	7.33	7.20	7.71	4.29
$[Zn_2(L^2)_2]^{4+}$	2.21	4.45	7.77	7.99	8.28	7.36	7.80	7.20	4.11, 3.86
$[Cd_2(L^2)_2]^{4+}$	2.36	4.34	8.18	8.04	8.34	7.53	7.12	6.56	3.10, 3.80
$[LuZn(L^2)_3]^{5+}$	2.16	4.21	7.74	7.86	8.17	7.63	7.25	5.34	3.54, 3.63
$[YZn(L^2)_3]^{5+}$	2.16	4.21	7.74	7.85	8.18	7.63	7.25	5.36	3.54, 3.63
$[LaZn(L^2)_3]^{5+}$	2.15	4.21	7.74	7.84	8.17	7.61	7.22	5.42	3.53, 3.64
$[CeZn(L^2)_3]^{5+}$	1.89	3.81	7.24	7.56	7.73	7.22	6.91	3.10	3.04, 3.15
$[PrZn(L^2)_3]^{5+}$	1.75	3.58	6.97	7.40	7.50	6.96	6.67	1.77	2.66, 2.87
$[NdZn(L^2)_3]^{5+}$	1.96	3.91	7.37	7.64	7.85	7.31	6.97	3.70	3.18, 3.22
$[SmZn(L^2)_3]^{5+}$	2.11	4.13	7.65	7.80	8.09	7.55	7.18	4.98	3.49, 3.53
$[EuZn(L^2)_3]^{5+}$	2.37	4.55	8.14	8.09	8.52	7.99	7.56	7.31	3.99, 4.16
$[TmZn(L^2)_3]^{5+}$	3.33	6.12	9.95	9.16	10.12	9.82	9.20	15.76	5.17, 6.27
$[YbZn(L^2)_3]^{5+}$	2.59	4.92	8.56	8.33	8.89	8.46	8.02	9.24	4.15, 4.61

Tridentate Binding Unit

compd	Me^3	H^9	H^{10}	H^{11}	H^{12}	H^{13}	H^{14}	$H^{15,16}$	$H^{17,18}$	Me^4	Me^5
L^2	4.21	7.69	7.23	7.34	8.38	7.93	7.57	3.61	3.35	1.30	1.13
$[Zn_2(L^2)_2]^{4+}$	4.20	6.06	7.33	7.56	8.49	8.57	8.19	3.62, 3.95	3.21, 3.42	0.73	1.43
$[Cd_2(L^2)_2]^{4+}$	4.31	6.94	7.15	7.57	8.57	8.45	8.07	3.20, 3.40	3.50, 3.70	0.94	1.43
$[LuZn(L^2)_3]^{5+}$	4.38	5.44	6.92	7.32	8.62	8.30	7.84	2.60, 2.77	3.43, 3.45	0.68	1.04
$[YZn(L^2)_3]^{5+}$	4.37	5.52	6.92	7.31	8.60	8.32	7.83	2.65, 2.78	3.41, 3.43	0.69	1.01
$[LaZn(L^2)_3]^{5+}$	4.33	5.82	6.96	7.35	8.52	8.35	7.82	2.84	3.34, 3.42	0.75	0.92
$[CeZn(L^2)_3]^{5+}$	5.27	−0.12	6.43	7.45	11.09	10.09	8.98	2.26, 3.03	3.47, 4.09	−1.23	1.28
$[PrZn(L^2)_3]^{5+}$	5.92	−3.72	6.12	7.75	12.98	11.09	9.89	2.04, 3.27	3.82, 4.83	−2.72	1.77
$[NdZn(L^2)_3]^{5+}$	5.00	1.68	6.56	7.97	11.29	9.90	9.37	2.55, 3.09	3.69, 4.15	0.90	1.39
$[SmZn(L^2)_3]^{5+}$	4.55	4.55	6.86	7.27	8.92	8.56	7.97	2.69, 2.75	3.40, 3.55	0.32	1.05
$[EuZn(L^2)_3]^{5+}$	3.75	9.89	7.42	6.06	4.60	6.34	5.46	2.59, 3.21	2.54, 2.91	2.67	0.38
$[TmZn(L^2)_3]^{5+}$	−0.13	33.50	8.95	6.63	−3.19	0.70	2.58	1.50, 3.24	−0.31, 3.84	11.86	−1.29
$[YbZn(L^2)_3]^{5+}$	2.57	16.12	7.63	7.09	4.52	5.88	6.10	1.93, 2.87	1.67, 3.31	5.20	−0.13

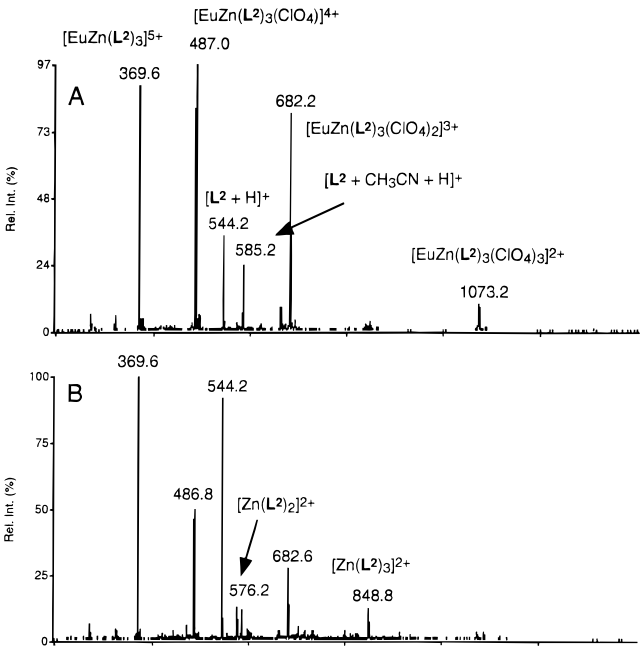

Figure 4. ES-MS spectra of $[EuZn(L^2)_3](ClO_4)_5$ (**10**) in acetonitrile for total ligand concentrations of (a) 10^{-4} M and (b) 10^{-5} M.

$(L^1)_2]^{4+}$ under similar conditions.[23] We have isolated $[Zn_2(L^2)_2](ClO_4)_4$ (**7**) by diffusion of diethyl ether into an acetonitrile solution in the form of white microcrystals, but we were unable to obtain crystals suitable for X-ray diffraction studies.

Heterodinuclear Complexes of L^2 with Zn(II) and Ln(III). ES-MS titrations of L^2(10^{-4} M) with an equimolar mixture of $Ln(ClO_4)_3 \cdot nH_2O$ (Ln = La, Eu, Gd, Tb) and $Zn(ClO_4)_2 \cdot 6H_2O$ in acetonitrile show the formation of only one heterodinuclear complex $[LnZn(L^2)_3]^{5+}$ and its adduct ions[35] with perchlorate (Table 1, Figure 4). These observations are confirmed by spectrophotometric titrations under similar conditions (total ligand concentration = 10^{-4} M; Ln = La, Eu; metal: L^2 = 0.1−1.1; metal concentration = Ln(III) concentration = Zn(II) concentration) which display a sharp end point for metal: L^2 = 0.33 combined with an isobestic point at 30 120 cm^{-1} (Figure 2c). Factor analysis[32] reveals the formation of only one absorbing complex in significant quantity, and the fit with equilibrium 8 readily converges with the following stability

$$Ln^{3+} + Zn^{2+} + 3L^2 \leftrightarrow [LnZn(L^2)_3]^{5+} \quad \log(\beta_{113}^{LnZn}) \qquad (8)$$

constants: $\log(\beta_{113}^{LaZn}) = 29.0(4)$ and $\log(\beta_{113}^{EuZn}) = 28.6(6)$ (RMS = 0.002). These values are only approximate since our model did not take into account the possible formation of minor quantities of the homonuclear complexes described in eqs 1−7. This simplification is justified by the existence of one isobestic point and by the ES-MS spectra which include peaks corresponding to the free ligand and to $[LnZn(L^2)_3]^{5+}$ only (Figure 4a). For a lower total ligand concentration (10^{-5} M), the spectrophotometric data are modified, displaying a complicated variation of the molar absorbances and two end points for metal: L^2 = 0.2 and 0.6. Attempts to fit the data were unsuccessful because the great similarity between the calculated absorption spectra of the complexes prevents the simultaneous fit of the eight equilibria 1−8. These data suggest however that the assembly of the heterodinuclear complexes $[LnZn(L^2)_3]^{5+}$ is almost quantitative at 10^{-4} M, but competition with homonuclear complexes occurs for lower concentrations. ES-MS spectra confirm this statement and show the formation of significant quantities of $[Zn(L^2)_3]^{2+}$ (*m*/*z* 847.8) and $[Zn(L^2)_2]^{2+}$ (*m*/*z* 575.8) associated with increasing fractions of free ligand for a total ligand concentration of 10^{-5} M (Figure 4b). At 10^{-6} M, only significant peaks corresponding to the free ligands are detected by ES-MS.

Slow diffusion of diethyl ether into a concentrated acetonitrile solution of the complexes $[LnZn(L^2)_3]^{5+}$ leads to the quantitative isolation of polycrystalline aggregates whose elemental analyses correspond to $[LnZn(L^2)_3](ClO_4)_5 \cdot 0.5Et_2O \cdot 2H_2O$ (Ln = La, **8**; Nd, **9**; Eu, **10**; Gd, **11**; Tb, **12**). The IR spectra are similar and display the characteristic vibrations of the heterocyclic ligands in the range 1570−600 cm^{-1} [41,47] together with an intense carbonyl stretching vibration assigned to the carboxamide group (1595 cm^{-1}) which is red-shifted with respect to the free ligand (1635 cm^{-1}). The ClO_4^- anions show the two vibrations (1095 and 625 cm^{-1}) typical of ionic perchlorates.[53]

Crystal Structure of $[EuZn(L^2)_3](ClO_4)(CF_3SO_3)_4(CH_3CN)_4$ (13). Fragile colorless single crystals of $[EuZn(L^2)_3](ClO_4)(CF_3SO_3)_4(CH_3CN)_4$ (**13**) suitable for X-ray diffraction analysis were obtained by diffusion of diisopropyl ether into an acetonitrile solution of **10** containing 30 equiv of $NBu_4CF_3SO_3$, followed by ultrasonic mixing and slow cooling to 277 K. A partial report of the crystal structure of this complex has already been published.[27] Selected bond lengths and angles are given in Table 4. Figure 5 shows the atomic numbering scheme, and Figure 6 gives an ORTEP[40] stereoscopic view of the complex perpendicular to the pseudo-C_3 axis.

The crystal structure of **13** consists of a $[EuZn(L^2)_3]^{5+}$ cation, five uncoordinated anions (one perchlorate and four triflates) and 4 solvent molecules. The anions and solvent molecules are disordered (see the Experimental Section). In $[EuZn(L^2)_3]^{5+}$, the three segmental ligands L^2 adopt a head-to-head arrangement[23,47] and are wrapped around a pseudo-C_3 axis passing through the metal ions (Eu···Zn = 8.960(3) Å). The three bidentate binding units are coordinated to Zn(II) while the three remaining tridentate units are bound to Eu(III), leading to a heterodinuclear triple-helical structure. Within each tridentate binding unit a, b, or c, the benzimidazole nitrogen atom N(4) and the oxygen atom O(1) coordinated to Eu(III) lie on the same side of the plane of the central pyridine ring (*i.e.*, the dihedral angles N(4)−C(20)−C(21)−N(6) and N(6)−C(25)−C(26)−O(1) are of opposite sign), leading to a bent conformation similar to that reported for L^4 in $[Eu(L^4)(NO_3)_3]$.[36] This produces a significant distortion of the screw thread for the tridentate units coordinated to Eu(III) which strongly contrasts with the usual regular wrapping observed for the analogous mononuclear $[Eu(L^3)_3]^{3+}$ [21,46] and dinuclear $[Eu_2(L^5)_3]^{6+}$ [41] complexes where the coordinated nitrogen atoms of the two distal benzimidazole rings lie systematically on the opposite side of the central pyridine ring. The coordination polyhedron of the Eu atom is a slightly distorted tricapped trigonal prism with the three N atoms of the benzimidazole units and the three O atoms occupying the vertices of the prism. The Eu−O and Eu−N bond distances are close to the standard values reported for Eu−O(amide),[25,54]

(49) Rüttimann, S.; Piguet, C.; Bernardinelli, G.; Bocquet, B.; Williams, A. F. *J. Am. Chem. Soc.* **1992**, *114*, 4230−4237.
(50) Constable, E. C.; Elder, S. M.; Healy, J.; Ward, M. D.; Tocher, D. A. *J. Am. Chem. Soc.* **1990**, *112*, 4590−4592.
(51) Epperlein, B. W.; Krüger, H.; Lutz, O.; Schwenk, A. *Z. Naturforsch. Teil A* **1974**, *29*, 1553−1557.
(52) Goodfellow, R. J. In *Multinuclear NMR*; Mason, J., Ed.; Plenum Press: New York and London, 1989; pp 566−577. Reger, D. L.; Myers, S. M.; Mason, S. S.; Rheingold, A. L.; Haggerty, B. S.; Ellis, P. D. *Inorg. Chem.* **1995**, *34*, 4996−5002.
(53) Nakamoto, K. *Infrared and Raman Spectra of Inorganic and Coordination Compounds*, 3rd ed.; J. Wiley: New York, Chichester, Brisbane, and Toronto, 1972; pp 142−154.
(54) Franklin, S. J.; Raymond, K. N. *Inorg. Chem.* **1994**, *33*, 5794−5804.

Table 4. Selected Bond Distances (Å) and Bond Angles (deg) for $[EuZn(L^2)_3](ClO_4)(CF_3SO_3)_4(CH_3CN)_4$ (**13**)

Distances				
		ligand a	ligand b	ligand c
Eu···Zn	8.960(3)			
Eu−O(1)		2.40(2)	2.37(1)	2.38(1)
Eu−N(4)		2.53(2)	2.58(2)	2.61(2)
Eu−N(6)		2.59(2)	2.65(2)	2.55(2)
Zn−N(1)		2.15(2)	2.19(2)	2.52(2)
Zn−N(2)		2.12(2)	2.01(2)	2.03(2)

Angles			
	bite angles		
	ligand a	ligand b	ligand c
N(1)−Zn−N(2)	78.2(7)	77.0(7)	74.0(7)
N(4)−Eu−N(6)	63.7(5)	62.9(5)	62.9(6)
N(6)−Eu−O(1)	63.7(5)	63.6(5)	63.9(5)
N−Zn−N			
N(1a)−Zn−N(2b)	96.2(7)	N(1a)−Zn−N(1c)	85.2(6)
N(1a)−Zn−N(2c)	159.1(7)	N(2a)−Zn−N(1b)	174.1(7)
N(2a)−Zn−N(2b)	105.6(7)	N(2a)−Zn−N(1c)	80.3(6)
N(2a)−Zn−N(2c)	96.4(7)	N(1a)−Zn−N(1b)	96.4(6)
N(1b)−Zn−N(1c)	97.2(6)	N(1b)−Zn−N(2c)	87.9(7)
N(2b)−Zn−N(1c)	174.1(6)	N(2b)−Zn−N(2c)	104.7(7)
N−Eu−N			
N(4a)−Eu−N(4b)	87.8(5)	N(6a)−Eu−N(6b)	117.8(6)
N(4b)−Eu−N(4c)	88.9(5)	N(6b)−Eu−N(6c)	120.7(6)
N(4a)−Eu−N(4c)	85.3(6)	N(6a)−Eu−N(6c)	120.6(6)
N(4a)−Eu−N(6c)	142.4(5)	N(4a)−Eu−N(6b)	74.2(5)
N(6a)−Eu−N(4b)	147.9(5)	N(4b)−Eu−N(6c)	72.9(5)
N(6b)−Eu−N(4c)	145.1(5)	N(6a)−Eu−N(4c)	75.0(6)
O−Eu−N			
N(4a)−Eu−O(1c)	143.9(5)	N(4a)−Eu−O(1b)	82.7(5)
N(6a)−Eu−O(1b)	67.4(5)	N(6a)−Eu−O(1c)	133.8(5)
N(6b)−Eu−O(1c)	69.7(5)	N(4b)−Eu−O(1c)	78.0(5)
O(1a)−Eu−N(6b)	134.8(5)	O(1a)−Eu−N(4a)	127.4(5)
O(1a)−Eu−N(4c)	80.0(5)	O(1a)−Eu−N(6c)	69.1(5)
O(1c)−Eu−N(4c)	126.8(6)	O(1a)−Eu−N(4b)	141.4(5)
O(1b)−Eu−N(4c)	142.1(5)	O(1b)−Eu−N(6c)	134.8(5)
O(1b)−Eu−N(4b)	126.3(5)		
O−Eu−O			
O(1a)−Eu−O(1b)	79.1(5)	O(1b)−Eu−O(1c)	79.6(5)
O(1a)−Eu−O(1c)	79.5(5)		

Eu−N(pyridine), and Eu−N(benzimidazole).[21,41,46] Zn(II) lies in a severely distorted octahedral site produced by the six N donor atoms of the three bidentate units. The Zn−N(1c) bond length (2.52(2) Å) is much longer than the standard Zn−N(pyridine) value (2.111 Å)[55] and than the average Zn−N distance in **13** (2.17 Å). As expected from the thermodynamic "trans influence",[56] the Zn−N(2b) bond (trans to Zn−N(1c)) is short (2.01(2) Å), which shifts N(1a) and N(2c) toward N(1c) (N(1a)−Zn−N(2c) = 159.1(7)°, Figure 6), leading to a Zn coordination sphere close to a distorted trigonal bipyramid if the loosely bond N(1c) atom is neglected. This distortion results from a close intermolecular packing of the $[EuZn(L^2)_3]^{5+}$ cations by pairs in the unit cell. Within each pair, the cations are disposed around an inversion center located on the side of the Zn atom. This situation leads to particular structural features between the two paired cations: (i) a parallel orientation of their pseudo-C_3 axes, (ii) a head-to-head arrangement with a short intermolecular Zn···Zn distance (8.315(4) Å), and (iii) a staggered packing of the 5-methylpyridine rings bound to Zn(II), leading to severe distortions of the bidentate coordinated units (Figure 7). The 5-methylpyridine ring of strand c is the more constrained, and this may explain the long Zn−N(1c) bond length. The pairs of cations (possessing opposite helicities) are packed in the unit cell with their pseudo-C_3 axis approximately parallel to the *ac* plane and forming an angle of 27° with the *c* axis.

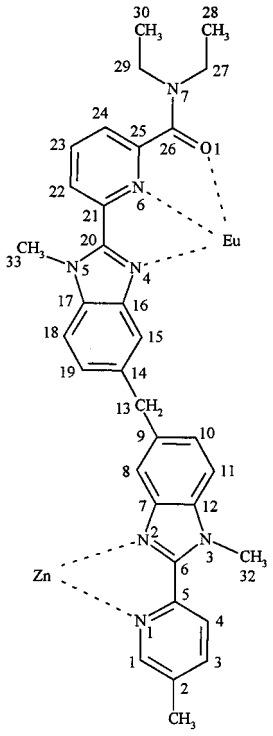

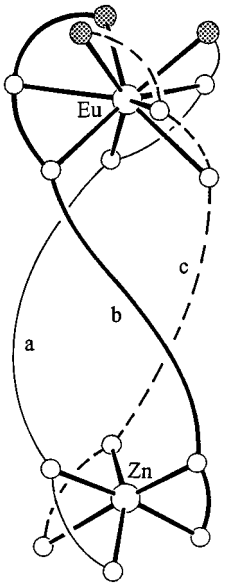

Figure 5. Atomic numbering scheme for $[EuZn(L^2)_3]^{5+}$ (**13**).

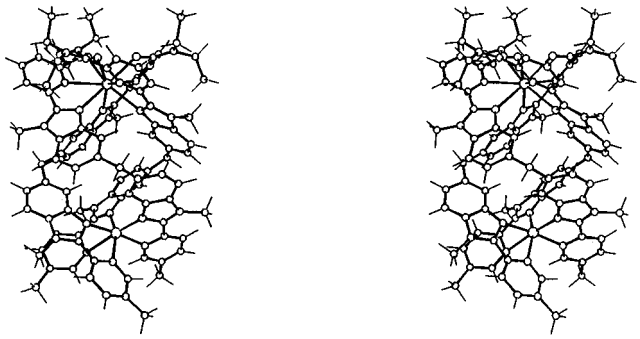

Figure 6. ORTEP[40] stereoview of the cation $[EuZn(L^2)_3]^{5+}$ perpendicular to the pseudo-C_3 axis in **13**.

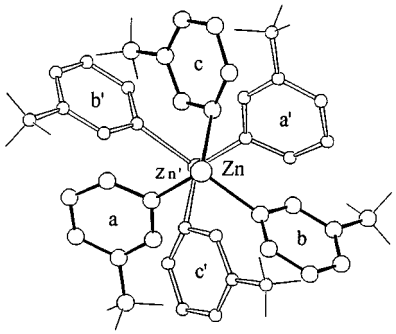

Figure 7. Packing of a pair of cations $[EuZn(L^2)_3]^{5+}$ around an inversion center showing their staggered arrangement in **13** (only the 5-methylpyridine groups bound to Zn(II) are represented).

Photophysical Properties of $[LnZn(L^2)_3]^{5+}$ (Ln = La, 8; La:Eu, 8a; Nd, 9; Eu, 10, 13; Gd, 11; Gd:Eu 11a; Tb, 12) in the Solid State. The reflectance spectrum of the free ligand

(55) Orpen, A. G.; Brammer, L.; Allen, F. H.; Kennard, O.; Watson, D. G.; Taylor, R. *J. Chem. Soc., Dalton Trans.* **1989**, S1−S83.

(56) Appleton, T. G.; Clark, H. C.; Maurer, L. E. *Coord. Rev.* **1973**, *10*, 335−422. Enemark, E. J.; Stack, T. D. P. *Angew. Chem., Int. Ed. Engl.* **1995**, *34*, 996−998.

Table 5. Ligand-Centered Absorption and Emission Properties in $[LnZn(L^2)_3]^{5+}$ Complexes in the Solid State[a]

compd	$\pi \rightarrow \pi^*$ (cm^{-1})		$^1\pi\pi^*$ (cm^{-1})		$^3\pi\pi^*$ (cm^{-1})			$\tau(^3\pi\pi^*)$ (ms)	
L^1 [b]		29 600	28 600 sh	25 000	19 200	18 650		719 ± 30	244 ± 43
$[LaZn(L^1)_3]^{5+}$ [b]		29 600	26 200	22 600	19 700	18 900		225 ± 32	84 ± 20
L^2		30 770		24 940[c]	20 040	18 870	17 860 sh	560 ± 18	41 ± 2
$[LaZn(L^2)_3]^{5+}$		31 000		22 600	19 960	19 050	18 000 sh	250 ± 4	36 ± 6
$[GdZn(L^2)_3]^{5+}$	32 800 sh	31 250	26 300 sh	22 600	19 960	19 050	18 000 sh	11.7 ± 0.1	5.04 ± 0.03
$[EuZn(L^2)_3]^{5+}$	32 750 sh	30 900	26 000 sh	21 480	*c*	*c*	*c*	*c*	*c*
$[TbZn(L^2)_3]^{5+}$	32 750 sh	30 900	26 400 sh	22 800	*c*	*c*	*c*	*c*	*c*

[a] Reflectance spectra recorded at 295 K, luminescence data at 77 K, and lifetime measurements at 10 K (λ_{exc} = 308 nm); sh = shoulder. [b] From ref 23. [c] $^3\pi\pi^*$ luminescence quenched by transfer to Ln ion.

L^2 displays one band at 30 770 cm^{-1}, assigned to a $\pi \rightarrow \pi^*$ transition,[57] which is slightly shifted upon complexation to yield either a very broad transition for $[LaZn(L^2)_3]^{5+}$ or a structured band centered at *ca.* 31 000 cm^{-1} with two shoulders around 32 000 and 26000−27000 cm^{-1} for the other heteronuclear complexes (Table 5, Figure F1 in the supporting information). Ligand L^1 displays somewhat similar spectra with a $\pi \rightarrow \pi^*$ transition split into two components separated by 1000 cm^{-1} in the uncomplexed state and by 3400−4500 cm^{-1} in the complexes. A weak luminescence is observed for L^2 at 77 K upon excitation of its singlet states: a structured band with a maximum at 24 900 cm^{-1} is assigned as arising from a $^1\pi\pi^*$ state while faint shoulders on the low-energy side (<20 000 cm^{-1}) are attributed to triplet state emissions. The latter assignment is supported by time-resolved luminescence measurements (Figure F2 in the supporting information): the singlet state emission is strongly reduced or even disappears when the delay time is set larger than 0.1 ms while the triplet state emission is still observed. It appears as a structured band with two maxima around 20 000 and 19 000 cm^{-1} and a shoulder around 18 000 cm^{-1}. The two maxima could be thought as originating from the two different nucleating parts of the ligand, but they may also be simply part of a vibrational progression (*ca.* 1000 cm^{-1}). The luminescence decay of the triplet state, measured at 10 K, is biexponential and typical of such $^3\pi\pi^*$ states (41 and 560 ms as compared to 244 and 719 ms for L^1).[23] Assignment of these lifetimes to a particular component of the triplet state emission was not possible because of the rather low intensity of the emission and of the small separation of the two components. There is however little doubt that these two lifetimes are associated with the two different coordinating segments of the ligand. Upon complexation to Zn(II) and Ln(III), the singlet state emission band shifts to lower energies (2200−3500 cm^{-1}) and a reduced intensity is observed for Eu and Tb as a result of the energy transfer between the ligand and the luminescent metal ions. For La and Gd, the triplet state emission is not significantly altered by the complexation, except for the lifetimes. Coordination of the metal ion perturbs the electron density of the ligand, henceforth the triplet state, facilitating nonradiative deexcitation paths and reducing the $^3\pi\pi^*$ lifetimes. The effect in $[LaZn(L^2)_3]^{5+}$ is similar to the one observed in the corresponding L^1 compounds.[23] The lifetime reduction measured for the paramagnetic $[GdZn(L^2)_3]^{5+}$ complex is substantially larger for both L^1 and L^2 (Table 5) and is the consequence of the proximity of the $^6P_{7/2}$ Gd(III) level (*ca.* 32 000 cm^{-1})[7] with the ligand singlet state.[21,23,41,58] Ligand L^2 displays a good antenna effect[2] since upon excitation through the $\pi \rightarrow \pi^*$ transition, the ligand-centered triplet state luminescence is completely quenched by efficient $^3\pi\pi^* \rightarrow$ Ln energy transfers to Nd, Eu, and Tb. Sharp emission bands arising from the Eu($^5D_0$) and Tb($^5D_4$) excited levels are observed at 77 and 10 K, while the metal-centered luminescence is totally quenched in the Nd-containing complex, the small $^4F_{3/2}-{}^4I_{15/2}$ gap (*ca.* 8000 cm^{-1})[7] favoring radiationless deexcitation processes.

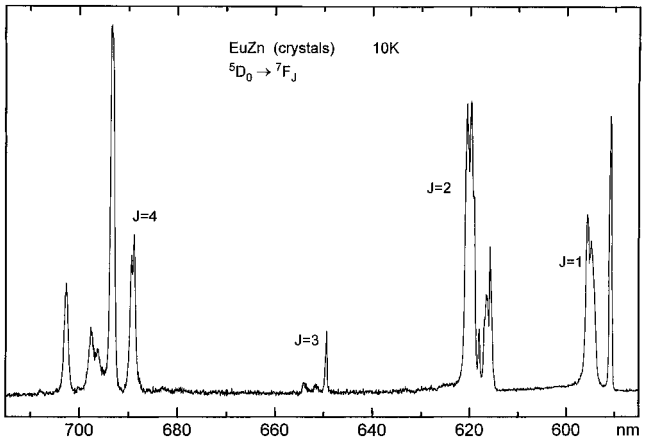

Figure 8. Emission spectrum of $[EuZn(L^2)_3](ClO_4)(CF_3SO_3)_4(CH_3CN)_4$ (**13**) measured at 10 K under excitation through the ligand levels (395 nm).

In contrast to the complexes with L^1, the Eu- and Tb-containing heteronuclear complexes with L^2 are strongly luminescent both in the solid state (at room or low temperature) and in solution. We have examined their properties in the solid state at 295, 77, and 10 K for the purpose of investigating the coordination environment around the luminescent ion, determining if the structure of the complexes changes along the series, and analyzing the energy migration pathways. At 10 K, the excitation spectrum of crystals of the Eu-containing compound **13** (Figure F3 in the supporting information) displays a broad and intense band with a maximum at 25 700 cm^{-1}, corresponding to excitation through the ligand $^1\pi\pi^*$ levels, and several sharp features arising from direct excitation onto the Eu(III) excited levels: ^5D_J (J = 0, 1, 2, 3) and $^5L_6$. The ligand excitation band extends below 400 nm in the spectrum of **13** while there is a sharp cutoff at this wavelength in the spectrum of the Tb-containing complex. Although the ligand-to-metal charge-transfer (LMCT) transition could not be formally evidenced, we note that the $^1\pi\pi^*$ ligand state in the Eu-containing heteronuclear complex lies at lower energy (1200−1400 cm^{-1}) than in the other complexes, indicating a possible mixing with the LMCT state (and eventually with some of the almost resonant f states). The emission bands obtained upon excitation either through the ligand states, with subsequent energy transfer to the ^5D_J manifold, or directly onto the $^5D_0$ level by use of a dye laser (Figure 8) are well resolved and typical of an emitting species containing a single lanthanide coordination environment with pseudotrigonal symmetry. In particular, the weak $^5D_0 \rightarrow {}^7F_0$ transition appears as a fairly symmetrical band centered at 17 220 cm^{-1} and with a full width

(57) Bochet, C. G.; Piguet, C.; Williams, A. F. *Helv. Chim. Acta* **1993**, *76*, 372−384.
(58) Alpha, B.; Ballardini, R.; Balzani, V.; Lehn, J.-M.; Perathoner, S.; Sabbatini, N. *Photochem. Photobiol.* **1990**, *52*, 299−306.

Table 6. Identified Eu(^7F_J) Crystal Field Levels (cm^{-1}, $J = 1-4$) in $[LnZn(L^2)_3]^{5+}$ Complexes, from Luminescence Spectra at 10 and 295 K, under Excitation through the Ligand Levels (**8a**, **10**, **11a**) or to the $^5D_0$ Level (**13**)

level	**13** (10 K)	**10** (295 K)	**8a** (295 K)	**11a** (295 K)	level	**13** (10 K)	**10** (295 K)	**8a** (295 K)	**11a** (295 K)
$^7F_1$	294	287	290	292	$^7F_3$	1824	1830	1834	1833
	411	399	411	394		1874	1881	1884	1888
	432	454	453	457		1931	1934	1927	1936
$^7F_2$	984	967	976	970	$^7F_4$	2706	2700	2706	2700
	1002	1016	1016	1019		2717	2742	2736	2741
	1043	1036	1036	1048		2799	2801	2800	2800
	1085	1094	1091	1090		2860	2841	2837	2838
	1107	1118	1124	1114		2888	2901	2892	2900
						2990	2999	2998	2998
$^5D_0$	17220	17229	17228	17226					

at half-height (fwhh) of 10 cm^{-1}. The corresponding $^5D_0 \leftarrow {}^7F_0$ excitation band is less symmetrical, and both its energy (17220−17229 cm^{-1}) and fwhh (9−15 cm^{-1}) depend upon the analyzing wavelength. This may reflect the simultaneous excitation of a crystal phonon with an energy of about 10 cm^{-1}. The breadth of the 0−0 transition points to crystals of relatively poor quality with defects resulting in different packing of the molecules and henceforth in somewhat different environments for the Eu(III) ions, as substantiated by the slightly different emission spectra obtained when the excitation wavelength is scanned through the 0−0 band profile. The low energy of the $^5D_0$ level is typical of Eu(III) coordinated to several heterocyclic N atoms[21,24,41,46] and suggests a large nephelauxetic effect.[7] The energy of the $^5D_0 \rightarrow {}^7F_0$ transition depends upon the ability of each coordinating atom to produce a nephelauxetic effect:[59] $\tilde{\nu} - \tilde{\nu}_0 = C_{CN}\sum_i n_i\delta_i$ where C_{CN} is a function of the total coordination number of the Eu(III) ion (1.0 for CN = 9), n is the number of i-type atoms, δ_i is the ability of the coordinating atom i to produce a nephelauxetic effect, and $\tilde{\nu}_0 = 17\,374$ cm^{-1} at 295 K (the temperature dependence of $\tilde{\nu}$ is approximately 1 cm^{-1} per 24 K).[1] The δ_i values are tabulated: −15.7 for an amide O atom and −12.1 for an amine N atom.[59] We have however recently demonstrated that a heterocyclic N atom (HN) tends to produce a larger nephelauxetic effect and have deduced from our work on complexes with benzimidazole-containing ligands a δ_{HN} parameter equal to −15.3. Taking the latter value into account, we predict an energy of 17 223 cm^{-1} for the $^5D_0 \rightarrow {}^7F_0$ transition of **13** at 10 K, a value only marginally different from the experimental finding, which confirms the correctness of the two nephelauxetic parameters. In addition to the low intensity of the $^5D_0 \rightarrow {}^7F_0$ transition, which is symmetry forbidden in D_3 but allowed in C_3 symmetry, detailed analysis of the $^5D_0$-excited emission spectrum of **13** (Figure 8, Table 6, Table SV in the supporting information) confirms the pseudotrigonal symmetry unraveled by the X-ray diffraction study. There are two main transitions to $^7F_1$, A → A and A → E, the latter being split into two components, indicating a deviation from the trigonal symmetry. The singlet/doublet pattern of the $^7F_1$ level has separations of 117 and 21 cm^{-1}, similar to the ones measured for $[Eu(L^3)_3]^{3+}$ (110 and 17 cm^{-1})[46] and for $[Eu_2(L^5)_3]^{6+}$ (118 and 18 cm^{-1}).[41] In the latter two compounds, the Eu(III) ion lies on a site with C_3 symmetry or close to it, meaning that the same situation prevails for $[EuZn(L^2)_3]^{5+}$ while the coordinating sites in $[EuZn(L^1)_3]^{5+}$ and $[Eu_2(L^5)_3]^{6+}$ display much larger distortions.[23] Analysis of the $^5D_0 \rightarrow {}^7F_2$ transition is less straightforward considering possible interferences with vibronic transitions.[1,41] This transition may however be viewed as comprised of two doublets (A → E, splittings 18 and 22 cm^{-1}) and of one, less intense singlet (A → A, $^7F_2$ sublevel at 1043 cm^{-1}), which is coherent with a pseudotrigonal symmetry, as are the six transitions observed to the $^7F_4$ level (six allowed in C_3 symmetry[1]).

When the $[EuZn(L^2)_3]^{5+}$ complex is measured as a powdered sample (**10**), the essential features of its luminescence spectrum are unchanged, especially the relative intensities of the transitions (Table SV in the supporting information), and the overall shape of the emission bands. The $^5D_0 \rightarrow {}^7F_0$ emission band is broader (fwhh = 20 cm^{-1} at 10 K) and displays a shoulder on its low-energy side, 10 cm^{-1} from the maximum which occurs at 17 231 cm^{-1}. Selective laser excitations within the profile of the 0−0 transition yield emission spectra with similar overall band shape and relative transition intensities, but differing in the fine splitting of the bands. In particular, the splitting of the $^7F_1$(E) crystal field sublevels is larger than for sample **13**, ranging from 37 to 68 cm^{-1}. Increasing the temperature to 295 K tends to favor the species deviating most from the idealized trigonal symmetry. Similar observations are made for the other crystal field sublevels. The solid aggregates **10** differ in chemical composition from the crystals **13** by their solvation molecules and by the counteranions: **13** contains weaker coordinating acetonitrile molecules, and in addition, four perchlorate anions are replaced by triflates. The differences observed between the emission spectra of **10** and **13** are reminiscent of the effects evidenced for the homonuclear complex with L^5: single crystals grown with acetonitrile as solvation molecules displayed highly symmetrical lanthanide coordination sites while introduction of water molecules in the lattice resulted in a lowering of the symmetry, as indicated by a larger $^7F_1$(E) splitting (41 cm^{-1} *vs* 18 cm^{-1}).[41] Since water molecules do not penetrate into the inner coordination sphere of the Eu(III) ion, the lifetime of the Eu($^5D_0$) level remaining unchanged, we concluded that the "solvation" effect in the homonuclear complex with L^5 resides in hydrogen bonding with the ligand strands, modifying the general coordination arrangement around the metal ions.[41] Therefore, the recorded excitation and emission spectra for **10** can be understood as reflecting the presence of several species in the aggregates, differing essentially by their solvation, henceforth by small distortions of the lanthanide ion environment consecutive to interactions of the ligand strands with the solvation molecules in the lattice.[60] Indeed, the Eu($^5D_0$) lifetimes are only marginally reduced (less than 10%) in going from sample **13** to **10**, while inner sphere coordination of a single water molecule would result in a dramatic decrease of this lifetime to less than 1 ms.[1] It is noteworthy that the luminescence measurements allow us to detect second-sphere effects, which demonstrates the utility of Eu(III) as a sensitive structural probe.

The luminescent properties of $[LnZn(L^2)_3]^{5+}$ complexes doped with 2% Eu(III) (Ln = La, **8a**; Gd, **11a**) are unchanged with respect to a pure Eu-containing powdered sample. At room

(59) Frey, S. T.; Horrocks, W. de W., Jr. *Inorg. Chim. Acta* **1995**, *229*, 383−390.

(60) Ligand dissociation (or rearrangement) in the excited state may be ruled out since it is not observed with crystals of **13**.

Table 7. Lifetimes of the Eu($^5D_0$) and Tb($^5D_4$) Excited Levels (ms) in $[LnZn(L^i)_3]^{5+}$ Complexes and Solutions under Various Excitation Conditions (Analyzing Wavelength Set on the Maximum of the $^5D_0 \rightarrow {}^7F_2$ or $^5D_4 \rightarrow {}^7F_5$ Transition)

compd	T (K)	λ_{exc} (nm)	τ (ms)
$[Eu_2(L^5)_3]^{6+}$ [a]	10	308	2.22 ± 0.07
$[EuZn(L^1)_3]^{5+}$ [a]	10	308	2.30 ± 0.05
$[EuZn(L^2)_3]^{5+}$ (**13**)	10	308	2.56 ± 0.10
		580.2	2.53 ± 0.10
		400	2.21 ± 0.30
$[EuZn(L^2)_3]^{5+}$ (**10**)	10	308	2.44 ± 0.03
		580.0	2.19 ± 0.01
		395	2.35 ± 0.02
	295	308	1.98 ± 0.01
		580.0	1.67 ± 0.02
		395	1.69 ± 0.01
$[(Gd:Eu)Zn(L^2)_3]^{5+}$ (**11a**)	10	308	2.29 ± 0.04[b]
		580.1	2.22 ± 0.01
	295	308	1.97 ± 0.08
10, 10^{-3} M in CH_3CN	295	308	2.56 ± 0.02
		580.0	2.59 ± 0.01
		392	2.72 ± 0.03
10, 10^{-4} M in CH_3CN	295	308	2.88 ± 0.01
		580.1	2.84 ± 0.05
		375	2.90 ± 0.02
$[TbZn(L^2)_3]^{5+}$ (**12**)	10	308	1.89 ± 0.06
		380	1.64 ± 0.01
		488.0	1.57 ± 0.02

[a] From ref 23. [b] The decay is biexponential. A second lifetime of 7.6 ± 0.3 ms can be extracted; it corresponds to the mean lifetime observed for the ligand-centered luminescence (see the text).

temperature, one single $^5D_0 \rightarrow {}^7F_0$ emission band appears at 17 228 (**8a**) and 17 226 (**11a**) cm^{-1} (Figure F5 in the supporting information), the overall shape of the emission spectra (Figure F4 in the supporting information) and the relative intensities of the $^5D_0 \rightarrow {}^7F_J$ ($J = 0-4$) transitions (Table SV in the supporting information) remain the same while the Eu($^5D_0$) lifetimes τ at 10 and 295 K in the Gd complex are identical to the ones measured for compound **10** (Table 7). The $^7F_1$(E) splitting amounts to 42 cm^{-1} for **8a** and to 63 cm^{-1} for **11a**, compared to an average of 55 cm^{-1} for **10** at room temperature. The increase of this splitting with the atomic number reflects the change in ionic radius, henceforth in Ln−N and −O distances, since shorter bond lengths generate stronger ligand-field effects. From these data, we conclude that $[LnZn(L^2)_3]^{5+}$ complexes (Ln = La−Gd) behave essentially as an isostructural series of compounds in which the lanthanide ions are well protected from external interactions. The Eu($^5D_0$) lifetimes are long, 2.5 ms at 10 K, in spite of the relative complexity of the ligand, which points to fairly rigid coordination sites. The ligand-to-europium energy transfer processes are rapid as a result of the good match between the ligand $^1\pi\pi^*$ and the Eu($^5L_6$,$^5D_3$) levels on one hand and the ligand $^3\pi\pi^*$ and the Eu($^5D_1$,$^5D_0$) levels on the other hand, leading to Eu($^5D_0$) lifetimes almost independent of the excitation mode. These lifetimes are somewhat longer than those measured with L^1, 2.22 ms for the homonuclear EuEu complex and 2.30 ms for the heteronuclear EuZn compound,[23] an effect consecutive to the coordination of the carboxamide group. In addition, the lifetime of the $^5D_0$ level and the total luminescence intensity (Table S5 in the supporting information) do not decrease much when the temperature is increased to 295 K. This points to a reduced influence of vibrational modes on the radiationless decay processes, contrary to what was reported for $[Eu(L^3)_3]^{3+}$ and $[Eu_2(L^5)_3]^{6+}$ for which τ decreases to *ca.* 0.3 ms at 295 K[41,46] and for the complexes with L^1 which are almost nonluminescent at room temperature.[23] Other interesting temperature effects occur: the Eu- and Tb-containing heteronuclear complexes **10** and **12** show the expected increase in luminescence intensity upon lowering the temperature from 295 to 10 K, but the increase amounts to a factor of 4 only for **10** while it is about 100-fold for **12**. Moreover, the Eu-doped La- and Gd-containing complexes **8a** and **11a** display an inverse temperature dependence, the luminescence intensity decreasing by a factor of 7−9 in going from 295 to 10 K. A temperature-mediated energy migration process occurs in these compounds, in which the energy taken up by the ligands migrates from one molecule to the other until it reaches an Eu-containing site, a phenomenon commonly observed in solid state samples doped with lanthanide ions.[61]

The Tb($^5D_4$) luminescence spectrum of complex **12** excited through the ligand level is dominated by the $^5D_4 \rightarrow {}^7F_5$ transition (Figure F6 in the supporting information) and the relative, corrected intensities of the $^5D_4 \rightarrow {}^7F_J$ transitions at 10 K are 1.0, 2.4, 0.9, 0.4, 0.04, 0.03, and 0.03 for $J = 6$, 5, 4, 3, 2, 1, and 0, respectively. The $^5D_4$ lifetime is shorter than the europium $^5D_0$ lifetime despite the larger $^5D_4-{}^7F_0$ gap compared to $^5D_0-{}^7F_6$, and it decreases with increasing temperature. This is a common feature of macrocyclic Tb-containing complexes[21,23,41,46,58] and is interpreted as revealing a Tb → ligand energy back-transfer, both the $^1\pi\pi^*$ and $^3\pi\pi^*$ states of the ligand lying close in energy to the $^5D_4$ terbium state.

Photophysical Properties of $[EuZn(L^2)_3]^{5+}$ in Acetonitrile Solution. The $\pi \rightarrow \pi^*$ transition of the ligand in solution appears at higher energy than in the solid state (2500 cm^{-1}) and is more red-shifted upon complexation (Table 2). All the heteronuclear complexes present an absorption maximum at 32 050 cm^{-1}, including the europium compound, the $\pi \rightarrow \pi^*$ transition of which does not display a larger red shift as observed in the solid state (*vide supra*). The excitation spectrum of $[EuZn(L^2)_3]^{5+}$ 10^{-4} M in acetonitrile displays a single, symmetrical, and relatively narrow band (fwhh = 25 nm) assigned to the ligand (Figure F3 in the supporting information). The luminescent properties of this solution are similar to those of the solid state samples: the overall shape of the spectrum and the relative intensities of the $^5D_0 \rightarrow {}^7F_J$ transitions (Table SV in the supporting information) match those of compounds **10** and **13**. Although the widths of the emission bands prevent a site symmetry analysis, there is no doubt that the pseudotrigonal arrangement of the triple helicate is maintained in solution, the $^5D_0 \rightarrow {}^7F_1$ transition appearing as one band with a shoulder and the $^5D_0 \rightarrow {}^7F_2$ transition as a doublet. The total emission intensity of a 10^{-3} M solution decreases by 40% upon saturation with oxygen (Figure F7 in the supporting information), which proves the role played by the ligand triplet state in the ligand-to-europium energy transfer, since dioxygen is known to quench the $^3\pi\pi^*$ state. The Eu($^5D_0$) lifetime is longer than in the solid state and increases upon dilution to reach 2.9 ms at 10^{-4} M (Table 7) where the concentration quenching becomes less important. The replacement of one benzimidazole unit by a carboxamide group leads to $[EuZn(L^2)_3]^{5+}$ solutions having a quantum yield 10^3 times larger than that of $[EuZn(L^1)_3]^{5+}$ solutions (Table 8), despite the rather similar photophysical properties of ligands L^1 and L^2. The only differences lie in a blue shift (*ca.* 2000 cm^{-1}) of the $\pi \rightarrow \pi^*$ transition, and in $^3\pi\pi^*$ states extending at slightly lower energy for compounds with L^2 (shoulders around 18 000 cm^{-1}, Table 5); this may promote a better energy transfer to the metal ion since the energy difference with $^5D_0$ is reduced. Moreover, radiationless deexcitation processes are less efficient in compounds with L^2, as indicated by the long and temperature-independent Eu($^5D_0$) lifetimes, a consequence of the more rigid metal ion environment provided by the carboxamide coordination. In fact, the total emission intensity, obtained by multiplying the quantum yield

(61) Blasse, G. *Prog. Solid State Chem.* **1988**, *18*, 79−171.

Table 8. Quantum Yields at 295 K of Anhydrous Acetonitrile Solutions Relative to $[Eu(terpy)_3]^{3+}$ (terpy = 2,2′:6′,2″-Terpyridine)

compd	concn (mol/dm^3)	added H_2O concn (mol/dm^3)	λ_{exc} (nm)	$\epsilon(\lambda_{exc})$ (M^{-1} cm^{-1})	rel quantum yield	rel emission intensity[a]
$[Eu(terpy)_3]^{3+}$	10^{-3}	0	390	71	1.00	1.00
	10^{-3}	0.18	390	71	0.87	0.87
	10^{-3}	0.93	390	71	0.27	0.27
	10^{-4}	0	380	119	0.60	1.00[b]
$[EuZn(L^1)_3]^{5+}$	10^{-3}	0	442	530	$\cong 1 \times 10^{-4}$	$\cong 7 \times 10^{-4}$
	10^{-4}	0	414	1960	$\cong 3 \times 10^{-4}$	$\cong 5 \times 10^{-3}$
$[EuZn(L^2)_3]^{5+}$	10^{-3}	0	395	555	0.13	1.02
	10^{-3}	0.93	395	555	0.13	1.02
	10^{-4}	0	380	2750	0.29	6.7
	10^{-4}	0.93	380	2750	0.29	6.7

[a] Product of the relative quantum yield multiplied by the ratio of the molar absorption coefficients ϵ(L)/ϵ(terpy) at the excitation wavelength used for measuring the emission of the heteronuclear complexes. [b] Taken as reference for 10^{-4} M solutions.

by the efficiency of light absorption (ratio of the molar absorption coefficients), is 6−7 times larger for the heteronuclear complex $[EuZn(L^2)_3]^{5+}$ compared with $[Eu(terpy)_3]^{3+}$ solutions. The efficient protection of the Eu(III) ion from solvent interaction is demonstrated by the addition of water to the solutions: the quantum yields remain constant up to a water concentration of 0.93 M, representing a 10^3-10^4 excess of H_2O, while the same addition to $[Eu(terpy)_3]^{3+}$ solutions results in a 63% reduction of the luminescence intensity and in a total loss of luminescence for $[EuZn(L^1)_3]^{5+}$.

Structure of the Complexes $[LnZn(L^2)_3]^{5+}$ (Ln = La, 8; Ce, 14; Pr, 15; Nd, 9; Sm, 16; Eu, 10; Tm, 17; Yb, 18; Lu, 19; Y, 20) in Acetonitrile. The ^1H NMR spectra of the diamagnetic complexes $[LnZn(L^2)_3]^{5+}$ (Ln = La, Lu, Y) show the quantitative formation of the heterodinuclear complexes in solution for the complete lanthanide series and display 23 signals arising from three equivalent ligands L^2 on the NMR time scale and compatible with C_3 or C_{3v} symmetry. The observed AB spin systems for the diastereotopic methylene protons $H^{7,8}$, $H^{15,16}$, and $H^{17,18}$ (Table 3) preclude the existence of mirror planes[49] leading to a C_3 head-to-head arrangement of the ligands in $[LnZn(L^2)_3]^{5+}$. The intrastrand NOEs observed for Me^2-H^3, Me^3-H^{12}, and $H^{14}-H^{17,18}$ (Figure 9) confirm that both the bidentate and tridentate binding units adopt cisoid conformation consecutive to their coordination to the metal ions while the NOEs experienced by the protons close to the methylene spacer (H^7-H^6, H^7-H^{10}, H^8-H^5, H^8-H^9, and H^6-H^9, Figure 9) are typical of the helical conformation of the ligands L^2 previously described for L^1 in $[LnZn(L^1)_3]^{5+}$ (Ln = La, Lu, Y).[23] The intramolecular closely packed triple-helical arrangement of the ligands in $[LnZn(L^2)_3]^{5+}$ (Ln = La, Lu, Y) is evidenced by (i) the significant upfield shift experienced by H^6 ($\Delta\delta$ = 2.29 ppm, Ln = La) and H^9 ($\Delta\delta$ = 1.87 ppm, Ln = La) which lie in the shielding region of the benzimidazole groups of the helically twisted ligands[23,47] and (ii) the weak interstrand NOEs observed for Me^4-Me^3, $H^{11}-H^4$, Me^3-H^5, and $H^{10}-Me^2$ as previously reported for $[LnZn(L^1)_3]^{5+}$ (Figure 9).[23] A careful comparison of the ^1H NMR spectra of $[LnZn(L^2)_3]^{5+}$ (Ln = La, Lu, Y, Table 3) shows that the contraction of the lanthanide radii only slightly affects the structure of the heterodinuclear complexes except for a small upfield shift of H^9 ($\Delta\delta$ = 0.30 ppm for Y(III), 0.38 ppm for Lu(III)) associated with a small distortion of the coordination sphere around Ln(III).[23]

Separation of Contact and Pseudocontact Contributions to the Paramagnetic Shifts in $[LnZn(L^2)_3]^{5+}$ (Ln = Ce, 14; Pr, 15; Nd, 9; Sm, 16; Eu, 10; Tm, 17; Yb, 18). Further structural and electronic information may be gained from the use of paramagnetic lanthanide metal ions as shift reagents.[48] The binding of the paramagnetic lanthanide ion *j* in $[LnZn(L^2)_3]^{5+}$ induces a frequency shift in the NMR signal of nucleus *i* given by the sum of the diamagnetic contribution δ_i^{dia} (taken from the chemical shift measured for the isostructural diamagnetic complexes $[LaZn(L^2)_3]^{5+}$ for Ce−Nd, $[YZn(L^2)_3]^{5+}$ for Sm−Dy, and $[LuZn(L^2)_3]^{5+}$ for Ho−Yb)[62] and the isotropic paramagnetic contribution δ_{ij}^{iso} which has two origins, the Fermi contact shift (δ_{ij}^{c})[63] and the pseudocontact (or dipolar) shift (δ_{ij}^{pc}):[64]

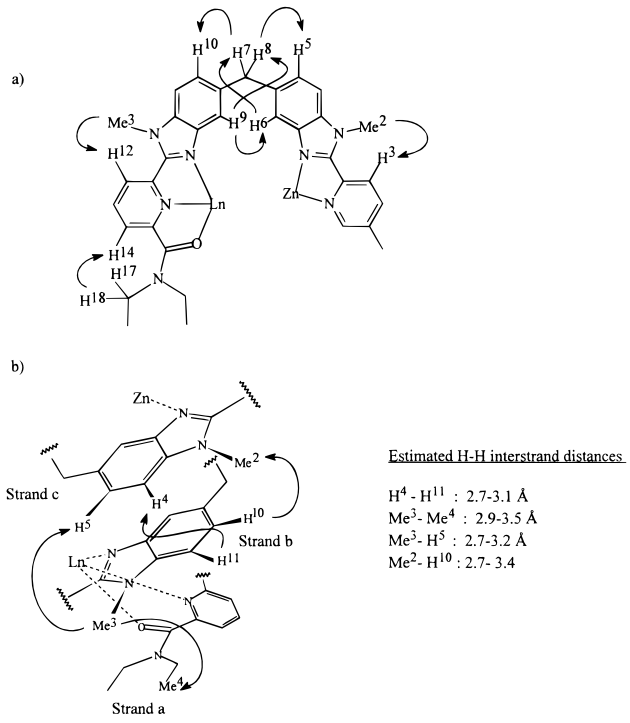

Figure 9. Selected (a) intrastrand and (b) interstrand NOEs observed for $[LnZn(L^2)_3]^{5+}$ (Ln = La, Ce, Pr, Nd, Sm, Eu, Yb, Lu, Y) in CD_3CN. Contact distances were calculated from the crystal structure of $[EuZn(L^2)_3](ClO_4)(CF_3SO_3)_4(CH_3CN)_4$ (**13**).

$$\delta_{ij}^{iso} = \delta_{ij}^{exp} - \delta_i^{dia} = \delta_{ij}^{c} + \delta_{ij}^{pc} \quad (9)$$

δ_{ij}^{c} results from through-bond Fermi contact interactions and is given by eq 10 where A_i is the hyperfine interaction parameter, $\mathbf{B}_0$ the applied magnetic induction, and $\langle S_z \rangle_j$ the expectation value

$$\delta_{ij}^{c} = \frac{A_i \cdot \langle S_z \rangle_j}{\hbar \cdot \gamma \cdot \mathbf{B}_0} = F_i \cdot \langle S_z \rangle_j \quad (10)$$

of S_z.[63] The pseudocontact shift δ_{ij}^{pc} depends on the geometric position of the nucleus *i* and results from the residual isotropic

(62) Kemple, M. D.; Ray, B. D.; Lipkowitz, K. B.; Prendergast, F. G.; Rao, B. D. N. *J. Am. Chem. Soc.* **1988**, *110*, 8275−8287.
(63) Golding, R. M.; Halton, M. P. *Aust. J. Chem.* **1972**, *25*, 2577−2581.
(64) Bleaney, B. J. *J. Magn. Reson.* **1972**, *8*, 91−100. Reuben, J.; Rigavish, G. A. *J. Magn. Reson.* **1980**, *39*, 421−430.

contribution associated with the anisotropic part of the molecular magnetic susceptibility tensor given by eq 11 for axial com-

$$\delta_{ij}^{pc} = \frac{1}{2N\hbar\gamma}(\bar{\chi} - \chi^{zz})_j \cdot \left(\frac{1 - 3\cos^2\theta_i}{r_i^3}\right) = G_i \cdot C_j \quad (11)$$

plexes.[62] R_i and θ_i are the internal polar coordinates of the nucleus i with respect to the ligand field axes, χ^{zz} is the axial component of the magnetic susceptibility tensor of a sample containing N paramagnetic ions, and $\bar{\chi} = (1/3)\cdot\mathrm{Tr}(\chi)$. Equations 10 and 11 show that the isotropic paramagnetic shift can be expressed as the sum of two contributions constituted by the product of two terms depending only on the lanthanide j and the nucleus i considered (eq 12).[65]

$$\delta_{ij}^{iso} = F_i \cdot \langle S_z \rangle_j + G_i \cdot C_j \quad (12)$$

Theoretical values of $\langle S_z \rangle_j$ and C_j have been reported[63,64] which allow the straightforward separation of contact and pseudocontact contributions using eq 12 and multilinear least-squares analysis[65] provided that (i) the system is axial (possessing at least a C_3 axis),[62] (ii) the various NMR signals of the nucleus i may be safely assigned for more than two paramagnetic Ln(III) ions, and (iii) the complexes $[LnZn(L^2)_3]^{5+}$ are isostructural. These conditions are fulfilled for Ln = Ce, Pr, Nd, Sm, Eu, Tm, and Yb since they possess a sufficiently short electronic relaxation time[48] to allow reliable 2D-COSY and NOEs to be detected, leading to the dependable assignment of the ^{1}H NMR signals given in Table 3. Moreover, the heteronuclear complexes possess a C_3 axis in solution and are almost isostructural as demonstrated by the similarity of the ^{1}H NMR spectra for the diamagnetic complexes $[LnZn(L^2)_3]^{5+}$ (Ln = La, Lu, Y) which cover the complete range of possible ionic radii in the lanthanide series.[6] Least-squares values for F_i and G_i, agreement factors for each proton (AF_i, eq 13)[65] and for each Ln(III) ion (AF_j, eq 13),[62] correlation coefficients for $\langle S_z \rangle_j$ versus

$$AF_i = \left[\frac{\sum_j (\delta_{ij}^{exp} - \delta_{ij}^{calc})^2}{\sum_j (\delta_{ij}^{exp})^2}\right]^{1/2} \quad AF_j = \left[\frac{\sum_i (\delta_{ij}^{exp} - \delta_{ij}^{calc})^2}{\sum_i (\delta_{ij}^{exp})^2}\right]^{1/2} \quad (13)$$

δ_{ij}^c (σ^c) and C_j versus δ_{ij}^{pc} (σ^{pc}),[65] and calculated corrected[65] contact and pseudocontact contributions are given in Table 9. The diastereotopic methylene protons have been excluded from the fitting process since no reliable attribution is possible for the separated signals of the AB spin systems.

The correlation coefficients and the agreement factors AF_i reported in Table 9 are satisfying ($0.07 < AF_i < 0.20$) and can be compared with those found for similar mathematical treatments applied to $[LnZn(L^1)_3]^{5+}$ ($0.08 < AF_i < 0.27$)[23] and [Ln(pyridine-2,6-dicarboxylate)$_3$]$^{3-}$ ($0.04 < AF_i < 0.27$).[65] As expected,[62,65] the contact contributions are negligible for spin delocalization on more than five bonds, leading to significant F_i values for H^9 and H^{11} to H^{14} only, which implies that Ln(III) is coordinated to the tridentate binding unit as found in the crystal structure of **13**. This is confirmed by the absolute G_i values which are maximum for H^6, H^9, and Me^4 and which point to short Ln−H distances (r_i) and large pseudocontact contributions (eq 11). The F_i values of the pyridine protons H^{12}−H^{14} are larger than those found for [Ln(pyridine-2,6-dicarboxylate)$_3$]$^{3-}$ ($F_i = 0.009-0.013$),[65] but similar to those reported for the analogous triple-helical complexes $[LnZn(L^1)_3]^{5+}$, demonstrating a significant spin delocalization onto the tridentate unit[23] induced by the coordination of the heterocyclic N donor atoms of ligands L^1 and L^2.

However, the agreement factors per Ln(III) (AF_j) are large and not satisfying even though we have not taken Sm(III) into account, since this ion induces negligible contact and pseudocontact shifts.[63,64] Kemple et al.[62] have shown that Bleaney's coefficients C_j[64] are poor approximations for the experimental molecular magnetic susceptibility tensors (χ) which must be measured if a better separation of contact and pseudocontact contributions is desired. We have therefore complied to the following procedure: (1) Internal spherical coordinates of the protons i were calculated from the crystal structure of $[EuZn(L^2)_3]^{5+}$ (**13**) with the Eu atom at the origin and the z axis corresponding to the pseudo-C_3 axis passing through the metal ions. According to the NMR data, axial C_3 symmetry is required in solution and C_3-averaged values of θ_i and r_i are used for the calculation of the structural factors $(1 - 3\cos^2\theta_i)/r_i^3$ (Table SIII in the supporting information). (2) Contact contributions were limited to protons remote from Ln(III) by at most five bonds, leading to only five significant contributions for H^9 and H^{11-14} in agreement with the calculated F_i values (Table 9). (3) The experimental paramagnetic isotropic shift of the aromatic protons H^n ($n = 1-6, 9-14$) were fitted using multilinear least-squares methods (12×6 fits)[62] to an expression analogous to eq 12 but containing only six parameters for each lanthanide j (eq 14). $\xi\chi_j^{zz}$ is the axial anisotropic susceptibility parameter

$$\delta_{ij}^{iso} = \xi \cdot \chi_j^{zz} \cdot \left(\frac{1 - 3\cos^2\theta_i}{r_i^3}\right) + \sum_{i=9,11-14} \delta_{ij}^{c} \quad (14)$$

of the lanthanide j in $[LnZn(L^2)_3]^{5+}$,[62] and δ_{ij}^c are the five significant contact contributions (Tables SVII and SVIII in the supporting information).

The agreement factors AF_j are significantly improved with this method ($0.007 < AF_j < 0.035$; Table SVII in the supporting information) and can be compared with those resulting from a similar mathematical treatment applied to [Ln(texaphyrin)(NO$_3$)$_2$] ($0.06 < AF_j < 0.26$).[66] Average F_i parameters may be calculated from the contact contributions (δ_{ij}^c) given in Table SVII in the supporting information (excluding Sm(III)) and using the spin expectation values tabulated by Golding and Halton.[63] They amount to $F_i = -0.33$ (H^9), 0.18 (H^{11}), 0.11 (H^{12}), 0.17 (H^{13}), and 0.10 (H^{14}), in qualitatively good agreement with the values reported in Table 9, which confirms the unusual large spin delocalization onto the coordinated tridentate binding units. Theoretical calculations[64] give estimates for the relative value of the axial term ($\xi\chi_j^{zz}$) of the magnetic susceptibility tensor for various Ln(III) with respect to Pr(III). Table 10 gives a comparison of the theoretical ratios[64] with the experimental values obtained for $[LnZn(L^2)_3]^{5+}$ (Ln = Ce, Pr, Nd, Eu, Tm, Yb) and using eq 11. Precise agreement is not expected due to (i) insufficient knowledge of the ion crystal field parameters, (ii) mixing of excited wave functions into the J manifold, (iii) nonideal colinearity of the principal axis of the magnetic susceptibility tensor and the molecular pseudo-C_3 axis, and (iv) possible distortions between the crystal structure and the structure in solution,[62] but we observe a qualitatively good agreement for the larger Ln(III) ions (Ln = Ce, Nd, Eu) and a significant deviation for Tm and Yb. These observations

(65) Reilley, C. N.; Good, B. W.; Desreux, J. F. *Anal. Chem.* **1975**, *47*, 2110−2116.

(66) Lisowski, J.; Sessler, J. L.; Lynch, V.; Mody, T. D. *J. Am. Chem. Soc.* **1995**, *117*, 2273−2285.

Table 9. Corrected Computed Values for Contact (δ^c)[a] and Pseudocontact (δ^{pc})[a] Contributions to the Experimental Isotropic Paramagnetic ^{1}H NMR Shifts for $[LnZn(L^2)_3]^{5+}$ Using Eq 12[65]

Bidentate Binding Unit

	Me^1	Me^2	H^1	H^2	H^3	H^4	H^5	H^6	AF$_j$[d]
F_i[b]	−0.015(8)	−0.02(1)	−0.03(1)	−0.017(9)	−0.02(1)	−0.02(1)	−0.019(6)	−0.14(7)	
G_i[c]	0.020(2)	0.033(3)	0.038(4)	0.022(2)	0.034(4)	0.038(2)	0.034(2)	0.17(2)	
AF$_i$[d]	0.14	0.13	0.15	0.14	0.15	0.09	0.07	0.15	
σ^c [e]	−0.993	−0.994	−0.993	−0.995	−0.993	−0.997	−0.998	−0.994	
σ^{pc} [e]	0.997	0.998	0.997	0.997	0.997	0.999	0.999	0.997	
δ^c(CeZn)[f]	−0.03	−0.04	−0.05	−0.03	−0.05	−0.03	−0.02	−0.26	0.44
δ^{pc}(CeZn)	−0.23	−0.36	−0.45	−0.25	−0.39	−0.36	−0.29	−2.06	
δ^c(PrZn)	−0.07	−0.10	−0.13	−0.08	−0.11	−0.09	−0.07	−0.66	0.33
δ^{pc}(PrZn)	−0.33	−0.53	−0.64	−0.36	−0.56	−0.56	−0.48	−2.99	
δ^c(NdZn)	−0.09	−0.13	−0.17	−0.09	−0.14	−0.12	−0.09	−0.80	0.18
δ^{pc}(NdZn)	−0.10	−0.17	−0.20	−0.11	−0.18	−0.18	−0.16	−0.92	
δ^c(SmZn)	0.00	0.01	0.01	0.00	0.01	0.00	0.00	0.03	0.67
δ^{pc}(SmZn)	−0.05	−0.09	−0.10	−0.05	−0.10	−0.08	−0.07	−0.41	
δ^c(EuZn)	0.14	0.23	0.27	0.16	0.23	0.22	0.18	1.33	0.14
δ^{pc}(EuZn)	0.07	0.11	0.13	0.08	0.11	0.14	0.13	0.62	
δ^c(TmZn)	0.12	0.20	0.24	0.14	0.20	0.19	0.15	1.16	0.02
δ^{pc}(TmZn)	1.05	1.71	1.97	1.16	1.75	2.00	1.80	9.26	
δ^c(YbZn)	0.04	0.06	0.07	0.04	0.06	0.06	0.05	0.34	0.11
δ^{pc}(YbZn)	0.39	0.65	0.75	0.43	0.66	0.77	0.72	3.56	

Tridentate Binding Unit

	Me^3	Me^4	Me^5	H^9	H^{10}	H^{11}	H^{12}	H^{13}	H^{14}
F_i[b]	0.04(3)	−0.07(7)	0.05(2)	−0.29(9)	−0.04(2)	0.123(6)	0.35(8)	0.17(6)	0.22(4)
G_i[c]	−0.081(7)	0.20(2)	−0.09(4)	0.49(5)	0.033(5)	0.005(1)	−0.17(2)	−0.12(2)	−0.07(1)
AF$_i$[d]	0.14	0.14	0.13	0.14	0.20	0.09	0.15	0.16	0.15
σ^c [e]	0.990	−0.931	0.994	−0.993	−0.991	0.997	0.996	0.994	0.996
σ^{pc} [e]	−0.997	0.992	−0.992	0.997	0.993	0.996	−0.997	−0.996	−0.997
δ^c(CeZn)[f]	0.07	−0.11	0.06	−0.50	−0.09	0.14	0.61	0.31	0.39
δ^{pc}(CeZn)	0.87	−1.87	0.30	−5.44	−0.44	−0.04	1.96	1.43	0.77
δ^c(PrZn)	0.19	−0.31	0.22	−1.32	−0.22	0.48	1.57	0.76	0.96
δ^{pc}(PrZn)	1.40	−3.16	0.63	−8.22	−0.62	−0.08	2.89	1.98	1.11
δ^c(NdZn)	0.23	0.04	0.27	−1.61	−0.23	0.65	1.89	0.93	1.20
δ^{pc}(NdZn)	0.44	0.11	0.20	−2.53	−0.17	−0.03	0.88	0.62	0.35
δ^c(SmZn)	−0.01	0.01	0.00	0.05	0.01	−0.03	−0.07	−0.03	−0.05
δ^{pc}(SmZn)	0.19	−0.38	0.04	−1.02	−0.07	−0.01	0.39	0.27	0.19
δ^c(EuZn)	−0.35	0.98	−0.49	2.68	0.39	−1.27	−3.37	−1.57	−2.12
δ^{pc}(EuZn)	−0.27	1.00	−0.14	1.69	0.11	0.02	−0.63	−0.41	−0.25
δ^c(TmZn)	−0.32	0.60	−0.38	2.37	0.34	−0.96	−2.82	−1.37	−1.76
δ^{pc}(TmZn)	−4.19	10.58	−1.95	25.69	1.69	0.27	−8.99	−6.23	−3.50
δ^c(YbZn)	−0.10	0.19	−0.15	0.70	0.09	−0.37	−0.79	−0.35	−0.48
δ^{pc}(YbZn)	−1.71	4.33	−1.02	9.98	0.62	0.14	−3.31	−2.07	−1.26

[a] Corrected contact and pseudocontact contributions are given in parts per million with $[LnZn(L^2)_3]^{5+}$ (Ln = La, Y, Lu) as diamagnetic references (see the text). [b] Contact term according to eq 12. [c] Pseudocontact term according to eq 12. [d] Agreement factors as defined in eq 13. [e] Correlation coefficients for contact and pseudocontact contributions (see the text).[65] [f] δ^c(LnZn) is the corrected[65] contact contribution in parts per million for the complex $[LnZn(L^2)_3]^{5+}$, and δ^{pc} is the corresponding pseudocontact contribution.

Table 10. Comparison of Theoretical and Experimental Values of the Principal Value of The Magnetic Susceptibility (χ) for $[LnZn(L^2)_3]^{5+}$ [a]

	theory[62,64]	experiment		theory[62,64]	experiment
CeZn	0.57	0.63	EuZn	−0.36	−0.54
PrZn	1.00	1.00	TmZn	−4.82	−2.86
NdZn	0.38	0.47	YbZn	−2.00	−1.07

[a] Ratios relative to Pr(III) are given.

suggest that the crystal structure of $[EuZn(L^2)_3]^{5+}$ (**13**) is a satisfying model for $[LnZn(L^2)_3]^{5+}$ in solution for lanthanide ions of similar sizes, but a contraction of the structure occurs to accommodate the smaller Ln(III) ions, as previously deduced from the upfield shift of H^6 and H^9 in the ^{1}H NMR spectrum of $[LuZn(L^2)_3]^{5+}$.

Discussion

The coordination behavior of L^2 with either d- or f-block metal ions is very complicated, leading to intricate mixtures of homonuclear complexes often difficult to characterize. The formation of four different complexes upon reaction of L^2 with Zn(II) ($[Zn(L^2)_3]^{2+}$, $[Zn(L^2)_2]^{2+}$, $[Zn_2(L^2)_3]^{4+}$, and $[Zn_2(L^2)_2]^{4+}$) contrasts with the formation of only two well-defined complexes with the analogous ligand L^1: $[Zn(L^1)_2]^{2+}$ in which Zn(II) is pseudooctahedrally coordinated by two tridentate binding units, and the head-to-head C_2 double helicate $[Zn_2(L^1)_2]^{4+}$ (structure **I**, Figure 3).[23] Moreover, the analogous complex $[Zn_2(L^2)_2]^{4+}$ adopts the alternating head-to-tail structure **II** (Figure 3) which demonstrates the different coordination behaviors displayed by ligands L^1 and L^2. This is confirmed by the intricate mixtures of homonuclear complexes which results from the reaction of L^2 with La(III) while only one thermodynamically assembled head-to-tail triple helicate $[La_2(L^1)_3]^{6+}$ is obtained under similar conditions with L^1.[23] Such features typically occur when the stereochemical requirements of the metal ion do not match the ligand binding capabilities.[33,67] For L^1, the tridentate and the bidentate binding units only differ in their denticity (the ligating imine nitrogen atoms and the chelate bite angle being the same), resulting in (i) a significant and similar affinity of both

(67) Constable, E. C. *Tetrahedron* **1992**, *48*, 10013−10059. Krämer, R.; Lehn, J.-M.; Marquis-Rigault, A. *Proc. Natl. Acad. Sci. U.S.A.* **1993**, *90*, 5394−5398.

Chart 2

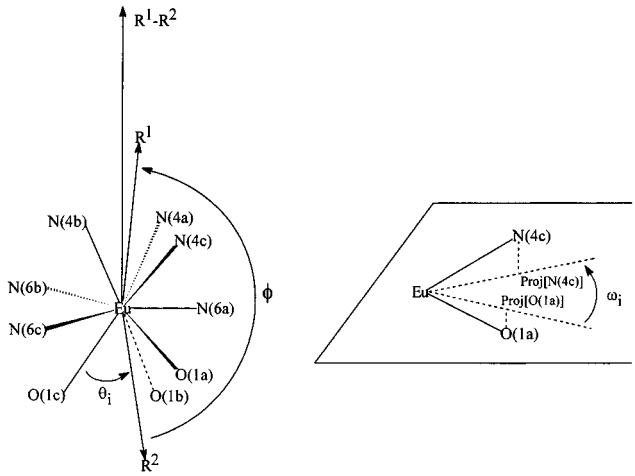

coordinating units for the same metal ion, (ii) the formation of stable and well-defined homonuclear complexes with either d- or f-block metal ions, and (iii) a limited thermodynamic selectivity for the formation of heterodinuclear d−f complexes. Only 45% of the heterodinuclear complex $[LaZn(L^1)_3]^{5+}$ is formed in acetonitrile when a 10^{-4} M solution of L^1 reacts with an equimolar mixture of La(III) and Zn(II).[23] The replacement of the terminal benzimidazole group of L^1 by an *N,N*-diethylcarbamoyl group produces a segmental ligand L^2 with two different binding units coded for one particular metal ion.[27] This leads to an opposite coordination behavior with the formation of intricate mixtures of homonuclear complexes and the quantitative formation of the heterodinuclear C_3 triple helicate $[LnZn(L^2)_3]^{5+}$ for a total ligand concentration of 10^{-4} M.

Although the assembly processes are strongly affected in going from L^1 to L^2, the heterodinuclear complexes $[LnZn(L^i)_3]^{5+}$ (i = 1, 2) display similar triple helical structures in solution with the three ligands wrapped about the C_3 axis passing through the metal ions. The three bidentate units are pseudooctahedrally coordinated to Zn(II), producing a noncovalent tripod which organizes the strands for the coordination of Ln(III). This thermodynamic control of the final structure prevents the facial−meridional isomerization and leads to a pure facial pseudotricapped trigonal prismatic arrangement of the tridentate binding units around Ln(III). In contrast with the systematic isolation of amorphous powders for the complexes of the lipophilic ligand L^1,[23] crystalline materials are obtained for the complexes $[LnZn(L^2)_3](ClO_4)_5$ (Ln = La−Lu), which allowed us to determine the crystal structure of the heterodinuclear complex $[EuZn(L^2)_3](ClO_4)(CF_3SO_3)_4(CH_3CN)_4$ (**13**). The triple-helical structure in the latter is slightly distorted by intermolecular packing interactions mainly affecting the coordination sphere around Zn(II). A detailed geometrical analysis of the coordination site occupied by Eu(III) was performed using the previously described[21] angles ϕ, θ_i, and ω_i (Chart 2, Table SIV in the supporting information; R^i is the sum of the vectors defining the two tripods of the trigonal prism: R^1 = Eu−N(4a) + Eu−N(4b) + Eu−N(4c) and R^2 = Eu−O(1a) + Eu−O(1b) + Eu−O(1c)[21]). The donor atoms O(1a), O(1b), and O(1c) of the carboxamide groups do not significantly affect the trigonal prismatic arrangement of the donor atoms of the tridentate units, resulting in structurally similar, slightly distorted tricapped trigonal prisms around Eu(III) for both $[EuZn(L^2)_3]^{5+}$ and $[Eu(L^3)_3]^{3+}$,[21] as reflected in the similar $^7F_1$(E) crystal field splittings (*vide supra*). The angle ϕ amounts to 178° for $[EuZn(L^2)_3]^{5+}$, which indicates that the two distal tripods are only slightly bent (ideal trigonal prism: ϕ = 180°), while the θ_i angles range between 47° and 54°, indicating a flattening along the pseudo-C_3 axis slightly more pronounced for the facial plane of the prism defined by the three oxygen atoms (Table SIV in the supporting information).

The structure is averaged in acetonitrile solution, in which axial C_3 triple-helical complexes $[LnZn(L^2)_3]^{5+}$ are observed on the NMR time scale with Zn(II) occupying the capping position. As recently discussed,[66,68] the separation of contact and pseudocontact contributions to the isotropic paramagnetic shifts for Ln(III) complexes is not an easy task, but crucial structural and electronic information results from such analysis. For the axial complexes $[LnZn(L^2)_3]^{5+}$, substantial simplifications occur,[62,65] and the method proposed by Reilley and co-workers[65] (eq 12) gives an approximate separation of contact and pseudocontact terms suitable for the dependable localization of Ln(III) ions in the tridentate binding units and the evaluation of spin delocalization onto the ligands. This first approach offers two advantages: (i) no prior knowledge of the structure other than axial symmetry around Ln(III) is needed and (ii) it allows a straightforward prediction (using eq 12 and the theoretical values of $\langle S_z \rangle_j$[63] and C_j[64]) of the paramagnetic shifts for Ln(III) ions not included in the fitting process. For instance, the assignment of the signals of the protons in $[TmZn(L^2)_3]^{5+}$ was confirmed using eq 12 and the parameters obtained from the fit with Ln = Ce, Pr, Nd, Sm, Eu, and Yb. However, we were unable to obtain dependable assignment of the 23 signals of $[TbZn(L^2)_3]^{5+}$ with this technique since the large errors associated with the calculated parameters F_i and G_i (10−30%, Table 9) preclude a suitable prediction for Tb(III), which possesses a large spin expectation value and a large Bleaney's coefficient compared to those used in the fitting process.[65] A more accurate separation of contact and pseudocontact contributions is obtained using eq 14 and the method of Kemple and co-workers.[62] It confirms that the triple helical structure found in the solid state for **13** is maintained in solution for the complete lanthanide series $[LnZn(L^2)_3]^{5+}$ (Ln = La−Lu) with a minor contraction for the heavy Ln(III) ions (Ln = Tm, Yb, and Lu). Significant contact contributions are observed for the aromatic protons bound to the tridentate binding units, suggesting an unusually large spin delocalization onto the ligands as reported previously for $[LnZn(L^1)_3]^{5+}$,[23] and in good agreement with the large nephelauxetic parameter associated with the heterocyclic nitrogen donor atoms coordinated to Eu(III) and determined from the $^5D_0 \rightarrow {}^7F_0$ excitation spectrum of $[EuZn(L^2)_3]^{5+}$.[23,64] Despite the improved agreement between experimental and calculated paramagnetic isotropic shifts, this second approach suffers from severe limitations: (i) prior knowledge of the molecular structure of the complexes is necessary and (ii) the prediction of paramagnetic isotropic shifts for the other Ln(III) ions is difficult since the magnetic susceptibility parameters ($\xi\chi^{zz}$) and the contact contributions are obtained by a least-squares fitting for each Ln(III) studied and no reliable extrapolation is possible.[62,68]

Analysis of the Eu($^5D_0$) luminescence in the solid samples shows the site symmetry of the lanthanide ion surprisingly less distorted with respect to a trigonal C_3 symmetry in the heteronuclear complexes with L^2 despite the replacement of one imine coordinating group in L^1 by an amide moiety, generating a nonhomogeneous coordination set of atoms in the tridentate binding unit. This relatively important structural difference generates few variations in the photophysical properties of the ligand L^2 with respect to L^1, but large changes in the luminescent properties of the Eu-containing heteronuclear complex $[EuZn(L^2)_3]^{5+}$. Although such changes were expected on the basis

(68) Lisowski, J.; Sessler, J. L.; Mody, T. D. *Inorg. Chem.* **1995**, *34*, 4336−4342. Forsberg, J. H.; Delaney, R. M.; Zhao, Q.; Harakas, G.; Chandran, R. *Inorg. Chem.* **1995**, *34*, 3705−3715.

of literature data which reveal the beneficial influence of carboxamide groups,[26a] they exemplify the fact that the observed emission results from second-order effects (f−f transitions are spin forbidden) and therefore that a small shift in the ligand electronic levels considerably influences the "resonant" energy transfer from the $^3\pi\pi^*$ state to the Eu($^5D_0$) level. In addition, the latter may be facilitated by the presence of the ν(C═O) vibration since the energy difference between the maximum of the emission band originating from the $^3\pi\pi^*$ state (ca. 19 000 cm^{-1} in the Gd-containing complex) and the $^5D_0$ level at 17 220 cm^{-1} corresponds roughly to one ν(C═O) phonon: for instance, an efficient ν(C═O) assisted radiationless energy transfer between Eu($^5D_1$) and Eu($^5D_0$) has been evidenced in europium perchlorate solutions in *N*,*N*-dimethylformamide.[69] Finally, the carboxamide group provides two additional features: (i) a more rigid Ln(III) environment (Ln−O distances are shorter than Ln−N bond lengths) favoring radiative deexcitation processes and therefore a longer Eu($^5D_0$) lifetime and (ii) a possible blue shift of the LMCT state, with respect to ligand L^1, as indicated by the temperature-independent Eu($^5D_0$) lifetime, leading to strong luminescence at room temperature, contrary to $[EuZn(L^1)_3]^{5+}$ which becomes nonluminescent when the temperature is raised. A similar shift has been invoked to explain the luminescence enhancement of Eu- and Tb-containing calix[4]arene complexes upon substitution of the phenol groups by alkylcarbamoyl functions,[26a] and of calix[8]arene[70] and substituted benzimidazole−pyridine[71] complexes upon replacement of the *p-tert*-butyl groups[70] and the (4-X-phenyl)pyridine moiety by electron-attracting nitro substituents. Finally, the resistance of the complexes toward hydrolysis, testified by the insensitivity of the luminescence total intensity with respect to water addition makes L^2 a promising step toward the synthesis of water-soluble and luminescent lanthanide triple helicates.

Conclusions

Most of the synthetic and specific molecular receptors developed so far for the selective complexation of Ln(III) ions had a cyclic structure in order to maintain the functional groups and the binding units in an appropriate orientation for them to easily coordinate the metal ions according to the *lock-and-key* concept.[72] However, more flexible acyclic receptors offer intrinsic advantages for the fine structural control often required for the recognition of guests as versatile as the lanthanide ions.[6] The new acyclic segmental ligand L^2 belongs to this second category, and its tridentate binding unit is coded for the selective coordination of Ln(III) ions[21,23] when the three stands are properly organized by the coordination of the bidentate binding units to a d-block metal ion. The spectroscopically inert Zn(II) is ideally suited for this purpose,[23] leading to a noncovalent tripod in $[LnZn(L^2)_3]^{5+}$ which controls the entropically-driven[9,41] formation of facial pseudotricapped trigonal prismatic lanthanide podates. This approach is relevant to biological recognition and regulation processes in which the tailored active site results from the specific preorganization of the polypeptidic backbone using various assembly processes based on noncovalent interactions such as hydrogen bonds, metal complexation, or van der Waals interactions.[73] The pseudotricapped trigonal prismatic lanthanide building blocks in the podates $[LnZn(L^2)_3]^{5+}$ are structurally similar to those found in $[Eu(L^3)_3]^{3+}$ and $[LnZn(L^1)_3]^{5+}$, but the replacement of the terminal benzimidazole groups by carboxamide substituents in L^2 strongly modifies the electronic properties of the tridentate binding units, leading to (i) an increased thermodynamic stability, (ii) a stronger luminescence of the Eu helicate $[EuZn(L^2)_3]^{5+}$ (10^3 more luminescent than $[EuZn(L^1)_3]^{5+}$), and (iii) an improved resistance toward hydrolysis. These points are crucial for the development of tailored luminescent probes and bioanalytical sensors,[1−3] but the new lanthanide podates $[LnZn(L^2)_3]^{5+}$ offer further fascinating possibilities for the preparation of molecular devices with predetermined physicochemical properties resulting from the judicious choice of spectroscopically and magnetically active d-block metal ions associated with Ln(III).[24,26]

Acknowledgment. We gratefully acknowledge Dr. Elisabeth Rivara-Minten, Ms. Véronique Foiret, and Mr. Bernard Bocquet for their technical assistance. C.P. thanks the Werner Foundation for a fellowship, and J.-C.G.B. thanks the Fondation Herbette (Lausanne) for the gift of spectroscopic equipment. This work is supported through grants from the Swiss National Science Foundation.

Supporting Information Available: Tables of atomic coordinates, bond distances, and bond angles for L^2 and $[EuZn(L^2)_3](ClO_4)(CF_3SO_3)_4(CH_3CN)_4$ (**13**), tables listing spherical coordinates for the protons in **13**, structural data obtained by a geometrical analysis of the europium coordination sphere, table of elemental analyses for complexes **7**−**12**, tables listing the luminescence intensities of complexes **8**−**13** under various experimental conditions, relative intensities of Eu($^5D_0 \rightarrow {}^7F_J$) and Tb($^5D_4 \rightarrow {}^7F_J$) transitions, tables listing the computed values of contact and pseudocontact contributions for aromatic protons and axial anisotropic magnetic susceptibility parameters for $[LnZn(L^2)_3]^{5+}$ using eq 14, and Figures F1−F7 showing reflectance, excitation, and emission spectra of complexes **8**−**13** (37 pages). See any current masthead page for ordering and Internet access instructions.

JA954163C

(69) Bünzli, J.-C. G.; Yersin, J.-R. *Helv. Chim. Acta* **1982**, *65*, 2498−2506.
(70) Bünzli, J.-C. G.; Ihringer, F. *Inorg. Chim. Acta* **1996**, *246*, 1−11.
(71) Petoud, S.; Bünzli, J.-C. G.; Piguet, C. Unpublished results.
(72) Lichtenthaler, F. W. *Angew. Chem., Int. Ed. Engl.* **1994**, *33*, 2364−2374.
(73) Voyer, N.; Lamothe, J. *Tetrahedron* **1995**, *51*, 9241−9284.